Finite Difference Neural Networks: Fast Prediction of Partial Differential Equations

Zheng Shi
Lehigh University
Bethlehem, PA 18015
zhs310@lehigh.edu

Nur Sila Gulgec
Thornton Tomasetti
San Francisco CA 94105
sgulgec@gmail.com

Albert S. Berahas
Lehigh University
Bethlehem, PA 18015
albertberahas@gmail.com

Shamim N. Pakzad
Lehigh University
Bethlehem, PA 18015
pakzad@lehigh.edu

Martin Takáč
Lehigh University
Bethlehem, PA 18015
takac.mt@gmail.com

Abstract

Discovering the underlying behavior of complex systems is an important topic in many science and engineering disciplines. In this paper, we propose a novel neural network framework, finite difference neural networks (FD-Net), to learn partial differential equations from data. Specifically, our proposed finite difference inspired network is designed to learn the underlying governing partial differential equations from trajectory data, and to iteratively estimate the future dynamical behavior using only a few trainable parameters. We illustrate the performance (predictive power) of our framework on the heat equation, with and without noise and/or forcing, and compare our results to the Forward Euler method. Moreover, we show the advantages of using a Hessian-Free Trust Region method to train the network.

1 Introduction

Partial differential equations (PDEs) are widely adopted in a plethora of science and engineering fields to explain a variety of phenomena such as heat, diffusion, electrodynamics, fluid dynamics, elasticity, and quantum mechanics, to mention a few. This is primarily due to their ability to model and capture the behavior of complex systems as well as their versatility. However, solving PDEs is far from a trivial task. Often incredible amounts of computing power and time are required to get reasonable results, and the methods used can be complicated and highly-sensitive to the choice of parameters.

The rapid development in data sensing (collection) and data storage capabilities provides scientists and engineers with another avenue for understanding and making predictions about these phenomena. The massive amounts of data collected from highly complex and multi-dimensional systems have the potential to provide a better understanding of the underlying system dynamics.

Utilizing this abundance of data to solve PDEs has been exploited in several recent studies; see e.g., [4, 6, 8, 12, 13, 16, 17, 19–21]. In [4, 21] and [19, 20], the authors applied symbolic regression and sparse regression techniques, respectively, to explain nonlinear dynamical systems. In [16, 17], the authors introduced physics informed neural networks using Gaussian processes. Moreover, Chen et al. [6] proposed continuous-depth residual networks and continuous-time latent variable models to train ordinary neural networks. Finally, in [8], the authors proposed conditional generative adversarial networks to predict solutions for steady state heat conduction and incompressible fluid flow, and, in

[12, 13], the authors proposed PDE-Net inspired by Wavelet theory to approximate the unknown nonlinear responses of diffusion and convection processes. Possibly the closest work to ours is PDE-Net [12, 13], which the authors proposed to learn differential operators by learning convolution filters. The key differentiating features of our approach can be summarized as follows: (i) our approach is computationally efficient since it trains finite difference inspired, small and linear filters; (ii) our network architecture can be adapted and enhanced to learn PDEs with forcing; and, (iii) we use a second-order optimization method to improve accuracy and computation time of training.

In this paper, inspired by finite-difference approximations and residual neural networks [9], we propose a novel neural network framework, finite difference neural networks (FD-Net), to learn the governing partial differential equations from trajectory data, and iteratively estimate future dynamical behavior. Mimicking finite-difference approximations, FD-Net employs "finite-difference" block(s) (FD-Block) with artificial time steps to learn first-, second- and/or higher-order partial derivatives, and thus learn the underlying PDEs from neighboring spatial points over the time horizon. As a proof-of-concept, we deploy our proposed method to learn and predict the underlying dynamics of PDEs using trajectory data from the heat equation in different cases: (1) simple homogeneous heat equation; (2) heat equation with noise; and, (3) heat equation with a forcing term.

Stochastic first-order methods have been very successful in training machine learning models in various applications [5]. However, there are several drawbacks to using such methods, and it has been shown that, for certain applications, employing stochastic second-order methods can be beneficial [1–3, 18, 23]. In this paper, we show that training our networks is one such application; training time can be significantly reduced and the accuracy of the solutions can be drastically improved by using a second-order method. Specifically, we employ a second-order Hessian-Free method, Trust-Region Newton CG [14, 22].

The paper is organized as follows. In Section 2, we introduce the PDE used in our case study and discuss the four different classes of problems that we investigate. We discuss in detail the fundamentals of FD-Net in Section 3. Extensive numerical results are presented in Section 4. Finally, in Section 5, we make some concluding remarks and discuss avenue for future research.

2 The Heat Equation

Consider a linear partial differential equation (PDE) in canonical form:
$$\mathcal{F}(x, t, u, u_t, u_x, u_{xx}, u_{xxx}, \dots) = 0, \tag{1}$$
where $\mathcal{F}$ is a linear function of u and its partial derivatives with respect to time and/or space. The objective of our study is to implicitly learn $\mathcal{F}$ given a series of measurements (trajectory data) at specific time and spatial instances, and predict the solutions to the equation throughout the time horizon.

For our case study, we consider the heat equation, one of the most frequently used PDEs in physics, mathematics, engineering and more. The heat equation describes the evolution of heat flow over time in an object [10]. Let $u(x, t)$ denote the temperature at a spatial point x and time t. The heat equation for a 1-D bar of length L can be expressed as
$$\frac{\partial u}{\partial t} = \beta \frac{\partial^2 u}{\partial x^2}, \tag{2}$$
where β is a rate of diffusion of the material. Under the assumption of perfectly insulated boundaries, the boundary conditions (BCs) can be expressed as
$$u(0, t) = 0, \qquad u(L, t) = 0. \tag{3}$$
We consider the following initial condition (IC)
$$u(x, 0) = \sum_{i=1}^{N} C_i \sin\left(\frac{i\pi x}{L}\right), \tag{4}$$
where $C_i \in \mathbb{R}$ for $i \in \{1, 2, ..., N\}$. The exact solution of (2) with BCs (3) and IC (4) can be expressed as
$$u(x, t) = \sum_{i=1}^{N} C_i \sin\left(\frac{i\pi x}{L}\right) e^{-\beta(i\pi/L)^2 t}. \tag{5}$$

The reasons we choose this PDE are three-fold: (1) it is an extensively used PDE that will allow us to investigate the merits and limitations of our proposed approach; (2) although the PDE is simple, it has several characteristics that are interesting to investigate (e.g., first- and second-order derivatives) and the behavior of the PDE can be complex in the presence of noise and/or a forcing term; and (3) we can derive the exact solution.

Given $x \in [0, L]$ and $t \in [0, T]$, (2) can be approximately solved via forward Euler method [7]. To this end, the domain is discretized (both in x and t) and $u(x, t)$ is computed recursively as follows:

$$u(x, t + \Delta t) = u(x, t) + \delta \left[u(x + \Delta x, t) - 2u(x, t) + u(x - \Delta x, t) \right], \quad \text{where } \delta = \beta \frac{\Delta t}{(\Delta x)^2}. \quad (6)$$

The performance of the Euler method, in terms of the accuracy of the solution, is highly dependent on the choice of the granularity of the discretization, both in time (Δt) and space (Δx). Specifically, the Euler method fails to generate accurate approximations, and may even diverge, if Δt and Δx do not satisfy $\delta \leq 0.5$, known as the stability criterion [15]. We should note that of course higher-order numerical procedures (or even implicit schemes) exist and could be used to solve (2) and mitigate some of the stability problems at the cost of more complex updates.

In addition to the instability associated with sparsely discretized time steps, in real-life applications the measurements of $u(x, t)$ are often contaminated with noise, e.g., Gaussian noise $\varepsilon \sim \mathcal{N}(\mu, \sigma^2)$, which can severely impact the stability and quality of the solutions. Moreover, the PDE could also have a forcing term, e.g.,

$$\frac{\partial u}{\partial t} = \beta \frac{\partial^2 u}{\partial x^2} + f(x), \qquad \text{where } f(x) = \sum_{i=1}^{N} D_i \sin \left(\frac{i \pi x}{L} \right), \quad (7)$$

and $D_i \in \mathbb{R}$ for $i \in \{1, 2, ..., N\}$. See Appendix A for the exact solution of (7).

The challenges that arise from instability, noisy measurements and forcing terms can make conventional approaches, such as the Euler method, vulnerable and result in inaccurate approximations. These challenges have inspired researchers in the fields of computational mathematics and machine learning to develop solution techniques that utilize the power of deep neural networks and exploit the massive amounts of measurements (i.e., trajectory data) that are readily available to solve PDEs and make predictions.

In this paper we investigate the performance of our proposed method, FD-Net, on the heat equation for all four aforementioned cases: (1) stable; (2) unstable; (3) noisy; and, (4) forced.

3 Fundamentals of FD-Net

In this section, we describe the fundamental components of FD-Net.

The building blocks of FD-Net are FD-Blocks, whose design is inspired by finite-difference approximations of partial derivatives. Figure 1 shows an instance of FD-Block. An FD-Block is a deep residual learning block [9] that aims to learn the evolution of a dynamical system for one artificial time step on $[t, t + \Delta t]$. It is composed of groups of convolutional layers, a fully connected (FC) layer, and a multi-step skip connection.

Specifically, for each group of convolutional layers, a certain number of "finite-difference" filters (FD-Filters) are defined in space: for $x \in \{\Delta x, 2\Delta x, ..., L - \Delta x\}$, the size of the filter is three (one parameter for x itself, one for its left neighbor and one for its right neighbor); for the boundaries, i.e., $x = 0$ or $x = L$, the size of a filter is two as there is only one neighbor, either on the left or right. The outputs of one group of layers with FD-Filters are concatenated to form a learned representation of partial derivatives of a certain order. In order to capture and mimic higher-order partial derivatives, multiple groups of convolutional layers with such filters are employed. The representation from a previous group is used as input of the subsequent group in order to learn a higher-order representation. The learned representations of partial derivatives, by all groups, are then concatenated and passed as input to the FC layer in order to learn the evolution (dynamics). Next, a skip connection is applied and the network proceeds to the following artificial time step.

Moreover, to imitate finite-difference approximations and to capture the behavior of linear equations, FD-Net defines the parameters of each layer without bias terms, and the outputs of the layers without applying nonlinear activation functions. In addition to the main architecture of the FD-Block, FD-Net
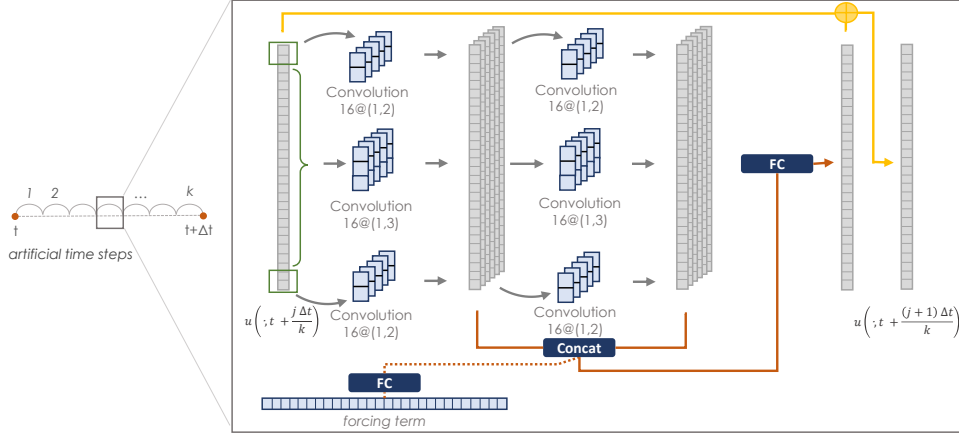
Figure 1: An illustration of FD-Block and the artificial time step. In this particular instance, there are k FD-Blocks defined in the network and thus $k - 1$ artificial time steps on $[t, t + \Delta t]$. For each FD-Block, there are 16 FD-Filters, two groups of convolutional layers, an FC layer, a forcing function representation and a skip connection. At the (artificial) time step $t + \frac{j\Delta t}{k}$ for $j = 0, 1, ..., k - 1$, the input $u(\cdot, t + \frac{j\Delta t}{k})$ is passed through the convolutional layers to learn the first- and second-order partial derivatives. Concatenated with the representation of the forcing function, the outputs are then passed through the FC layer with the skip connection to predict the function behavior at $t + \frac{(j+1)\Delta t}{k}$.

constructs a learnable representation via an FC layer and concatenates it with the outputs of the convolutional layers to learn forcing functions that are potentially present in the PDE.

Overall, FD-Net is formed by stacking multiple FD-Blocks sequentially in order to produce an approximate solution of the PDE at $t + \Delta t$ given a solution at t. Incorporating $k\,(>1)$ FD-Blocks introduces $k - 1$ artificial time steps between t and $t + \Delta t$ to FD-Net, which enhances the learning capability of FD-Net, especially when Δt is large. We discuss this further in Section 4. The number of FD-Blocks is the first hyper-parameter of FD-Net.

Furthermore, instead of defining distinct FD-Filters for each FD-Block, FD-Net shares the same FD-Filters along the sequence. As a result, the size of an instance of our networks does not depend on the number of FD-Blocks but rather on the number and size of the FD-Filters. FD-Net uses the same number of FD-Filters across all convolutional layers for a consistent input/output shape. We use this quantity as the second hyper-parameter of FD-Net and refer to it as "the number(s) of FD-Filters".

Table 1 shows the sizes of the networks, for different numbers of FD-Filters, used to learn PDEs with first- and second-order partial derivatives. Our experiments (see Section 4) indicate that 16 FD-Filters are sufficient for FD-Net to produce predictions with high precision for our case-study PDE for all aforementioned cases.

Table 1: Number of Parameters in FD-Net.

# FD-Filters	4	8	16	32	64
# Parameters w/o forcing[†]	148	520	1936	7456	29248
# Parameters[‡]	468	840	2256	7776	29568

[†] does not count parameters for learning forcing function.
[‡] includes all parameters in an instance of FD-Net, the forcing function is in the form of (7) with $N = 10$, $x \in [0, \pi]$ and $\Delta x = 0.1$.

4

4 Numerical Experiments

In this section, we present numerical experiments to demonstrate the empirical performance of `FD-Net` on the heat equation under the four scenarios described in Section 2: (1) stable case; (2) unstable case; (3) noisy case; and, (4) forcing case. We first describe the data we used in our experiments, then discuss the optimization methods employed for training the networks and finally show numerical results.

The main goal of the experiments is to study if `FD-Net` is capable of making accurate predictions throughout the time horizon by solely relying on trajectory data and iteratively learning the short-term (i.e., between t and $t + \Delta t$) evolutions. We illustrate the training and testing (prediction) performance of our proposed approach, compare the predictions made by `FD-Net` with the approximate solutions generated by the forward Euler method, demonstrate the advantages of training our networks with Trust-Region (TR) Newton CG method, and investigate the sensitivity of our networks to the hyper-parameters. For brevity, we show only a subset of our results in the main paper and defer the full experimental results to Appendix B.

4.1 Data, Training and Testing

For each aforementioned case, we generated synthetic data using the exact solutions to the heat equations; see Section 2. Specifically, for each case, we generated 200 different trajectories, each with a randomly generated initial condition, i.e., $C_i \sim \mathcal{N}(0,1)$, for $i \in \{1, 2, ..., 10\}$ in (4). We considered the 1D bar of length $L = \pi$, and the rate of diffusion parameter was set to $\beta = 2 \cdot 10^{-4}$. We set the spatial discretization to $\Delta x = 0.1$ on $[0, \pi]$, the time horizon as $[0, 1000]$, and the temporal discretization to $\Delta t = 1$ (namely, $\delta = 0.02 < 0.5$ in (6)), for the stable, noisy and forcing cases, and $\Delta t = 200$ (namely, $\delta = 4 > 0.5$ in (6)), for the unstable case. For the noisy case, we considered multiplicative noise of the form $u(x, t) = u(x, t)(1 + \gamma_i \epsilon_{x,t})$ for $i \in \{1, 2, 3\}$, where $\epsilon_{x,t} \sim \mathcal{N}(0, 1)$, and $\gamma_1 = 10^{-8}$ (low), $\gamma_2 = 10^{-4}$ (medium) and $\gamma_3 = 10^{-2}$ (high). For the case with a forcing function, we generated the function with $D_i \sim \mathcal{N}(0, 1)$ for $i \in \{1, 2, ..., 10\}$ in (7) and applied it to the PDEs of all initial conditions.

Let

$$A = \{u_s(x, t) \mid s \in S, \ x \in \{0, \Delta x, ..., L\}, \ t \in \{0, \Delta t, ..., T\}\}$$

denote a randomly generated data set, where S is the index set of ICs, $u_s(x, t)$ is the data (of measurements) and $\{u_s(x, t)\}_{x,t}$ is the trajectory data for a specific IC. We randomly selected 150 ICs as our training set, and the remainder (50 ICs) were used for testing purposes. We denote S_{train} and S_{test} the subsets of indices of ICs for training and testing, respectively.

For training purposes, we adopted a "one-step ahead" procedure. Let

$$A_{\text{train}} = \{(u_s(x, t), u_s(x, t + \Delta t)) \mid s \in S_{\text{train}}, \ x \in \{0, \Delta x, ..., L\}, \ t \in \{0, \Delta t, ..., T - \Delta t\}\}$$

define the training data set, where $(u_s(x, t), u_s(x, t + \Delta t))$ is a training tuple (sample), $u_s(x, t)$ is the input and $u_s(x, t + \Delta t)$ is the target. We defined the MSE loss of the stochastic mini-batch as

$$\text{MSE}_{\text{mini}} = \frac{1}{|A_{\text{mini}}|} \sum_{s, x, t} \left(u_s(x, t + \Delta t) - \tilde{u}_s(x, t + \Delta t)\right)^2, \tag{8}$$

where $A_{\text{mini}} \subseteq A_{\text{train}}$ is a mini-batch and $\tilde{u}_s(x, t + \Delta t)$ is the output of a network. On the other hand, for testing, we used a "1000-step" sequential prediction procedure (and refer to it as "1000-step prediction"). Let

$$A_{\text{test}} = \{(u_s(x, 0), u_s(x, T)) \mid s \in S_{\text{test}}, \ x \in \{0, \Delta x, ..., L\}\}$$

define the testing data set, $u_s(x, 0)$ be the input and $u_s(x, T)$ be the target. We used $u_s(x, 0)$ as the initial input and sequentially made predictions through the time horizon until reaching T, where the final prediction $\tilde{u}_s(x, T)$ was made. Specifically, $u_s(x, 0)$ was used as the input to make the next prediction $\tilde{u}_s(x, \Delta t)$, which in turn was used as the input to make the next prediction $\tilde{u}_s(x, 2\Delta t)$, and this was repeated throughout the whole time horizon. The error metric we used was MSE and was defined as

$$\text{MSE}_{\text{test}} = \frac{1}{|A_{\text{test}}|} \sum_{s, x} \left(u_s(x, T) - \tilde{u}_s(x, T)\right)^2. \tag{9}$$
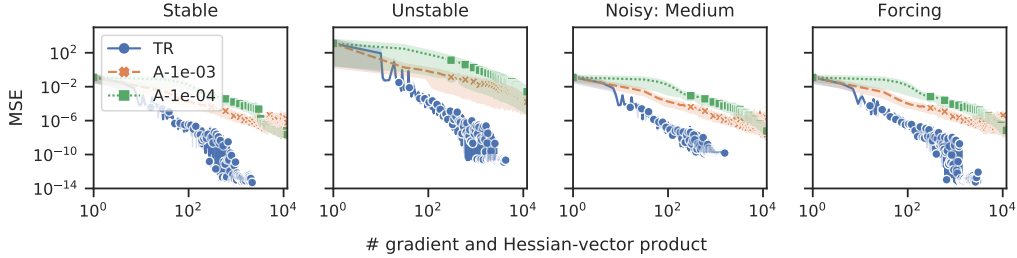
5

Figure 2: Evolution of training error. The marked dashes represent the average mini-batch MSE loss over 10 random seeds and the filled areas represent their 95% confidence intervals.

For each case, we configured the networks with different numbers of `FD-Blocks` and `FD-Filters` and used two optimization methods, ADAM (with learning rates 10^{-3} and 10^{-4}) [11] and Trust-Region (TR) Newton CG method [14], both with mini-batch sizes of 64. We prescribed a fixed budget of 100 iterations for the TR method on the stable, noisy and forcing cases and 300 iterations on the unstable case, but allowed the ADAM algorithm to run for 12000 iterations on all cases. For each configuration, algorithm and case, we used 10 random seeds to initialize network parameters and to generate stochastic mini-batches.

4.2 Results and Discussion

In this section, we present numerical results and discuss the strengths and limitations of `FD-Net`. We consider all the aforementioned cases: (1) stable; (2) unstable; (3) noisy (medium); and (4) forcing. For brevity, among all configurations investigated, we show results for the best configuration for each case (from an average performance perspective given the budget). Specifically, we show results for 1 `FD-Block` & 16 `FD-Filters` for the stable, forcing and noisy cases, and 10 `FD-Blocks` & 16 `FD-Filters` for the unstable case. Furthermore, we investigate the sensitivity of `FD-Net` to the hyper-parameters, i.e., numbers of `FD-Blocks` and `FD-Filters`. More numerical results with different numbers of `FD-Blocks` and `FD-Filters` and different noise levels can be found in Appendix B.

We begin our presentation by showing the evolution of the training errors, i.e., MSE_{mini} (8), for different optimization algorithms in Figure 2. We compare the performance of the algorithms in terms of the number of gradient and Hessian-vector computations. As is clear from the figure, the TR methods is able to achieve smaller MSE_{mini} than ADAM within the given budget for all cases. This is true for other `FD-Block` and `FD-Filter` configurations, as well as different noise levels; see Appendix B for more results.

Having demonstrated that our networks can be adequately trained within a budget, we proceed to show the testing (prediction) accuracy of `FD-Net` and compare against a standard benchmark numerical scheme, the forward Euler method, in Figures 3 and 4. Figure 3 shows the sequence of predictions made by `FD-Net`, for the stable case, at 5 time steps in the horizon. For brevity, in Figure 4, we only show the final predictions at $t = 1000$ for the remaining cases and defer the rest of the results to Appendix B. We chose the sequences of 1000-step predictions with the minimum testing errors (9) over the course of training, and compared them with the predictions made by the forward Euler method. We show results for a single IC. Figures 3 and 4 clearly indicate that: (1) `FD-Net`, when trained sufficiently well, is able to make higher quality predictions across the time horizon than the forward Euler method; (2) training our networks with the TR method allows for better predictions than the ADAM optimizer; (3) the performance of the forward Euler method is highly dependent on the case. Specifically, the Euler method, as predicted by the theory, cannot adequately capture the dynamics of the PDE in the unstable setting.

To further illustrate the testing (prediction) performance of `FD-Net`, in Figure 5, we show the minimum testing errors over the training process and the final testing errors for every case, algorithm and random seed. Clearly, training `FD-Net` using the TR method results in higher accuracy predictions with lower variance for all cases. Indeed, this is true for all configurations of `FD-Net`; see Appendix B.
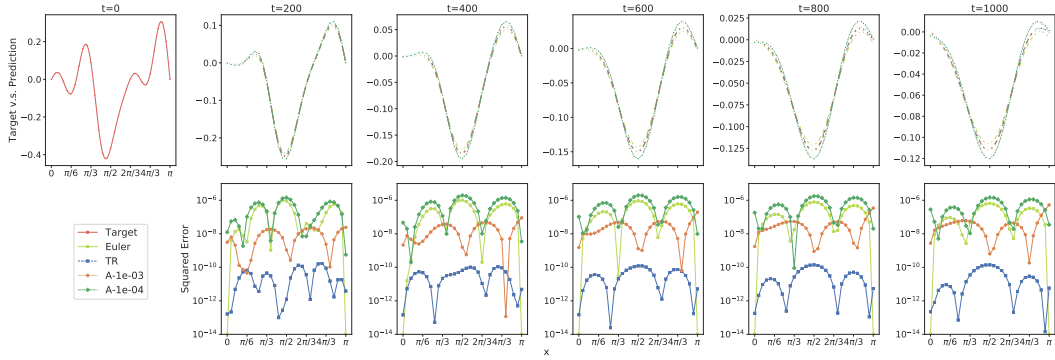
Abbreviation: Euler, forward Euler method.

Figure 3: Sequence of predictions for the stable case at $t \in \{200, 400, 600, 800, 1000\}$ and $x \in \{0, \Delta x, 2\Delta x, ..., \pi\}$ for one specific IC. Top Left corner: $u_s(x, 0)$; Rest of top row: Targets $(u_s(x, t))$ and predictions $(\tilde{u}_s(x, t))$; Bottom row: Squared errors $((u_s(x, t) - \tilde{u}_s(x, t))^2)$.
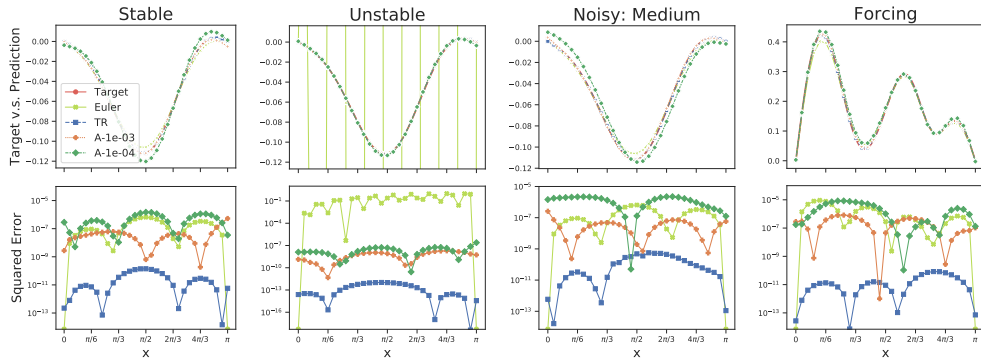
Figure 4: Final predictions for all cases at $t = 1000$ and $x \in \{0, \Delta x, 2\Delta x, ..., \pi\}$ for one specific IC. Top row: Targets and predictions; Bottom row: Squared errors.
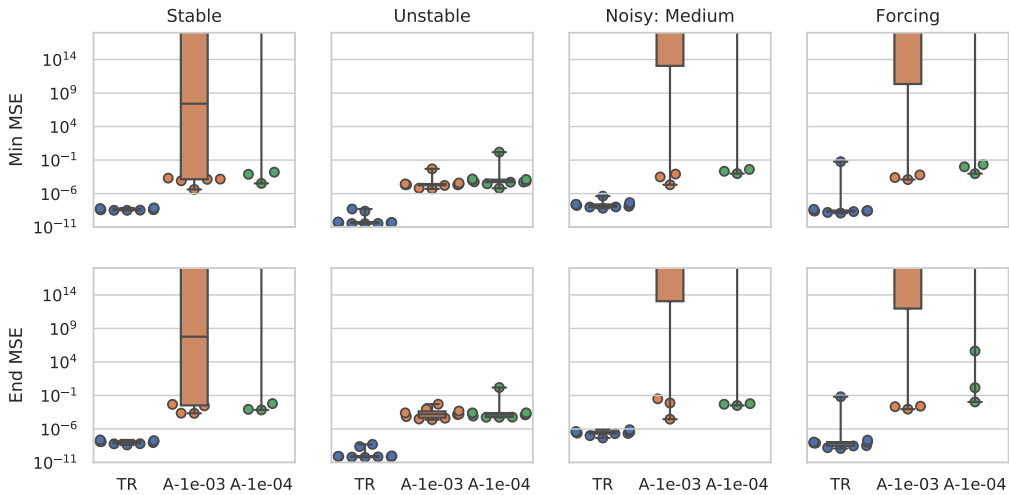
Figure 5: Testing error for different cases, algorithms and random seeds. Top row: Minimum testing error; Bottom row: Final testing error. Top/middle/bottom line of boxplot is the upper quartile/median/lower quartile, respectively, the whiskers represent the range, and the circled dots are individual observations.

It is worth noting that 1000-step prediction is a challenging task. This can be attributed to the fact that the error at each time step propagates throughout the time horizon, and any imperfect intermediate predictions can severely deteriorate the final prediction at $t = 1000$. This is evident for the networks trained by ADAM for the stable, noisy and forcing cases, where the testing errors for certain random seeds are very large. This effect is less severe for the unstable case as there are far fewer time steps from $t = 0$ to $t = 1000$. We should note, however, that the TR method is able to reduce the testing errors for all cases, and the effect of error propagation is not evident. This is true across the different cases so long as the networks are appropriately configured; see Appendix B for more details.

Next, we investigate the sensitivity of FD-Net to choices of the hyper-parameters (the numbers of FD-Blocks and FD-Filters). The main results are given in Figures 6 and 7; see Appendix B for more results. To fully reveal the learning capabilities of FD-Net, we used the TR method without imposing any budget, and trained the network of each configuration with 10 random seeds.
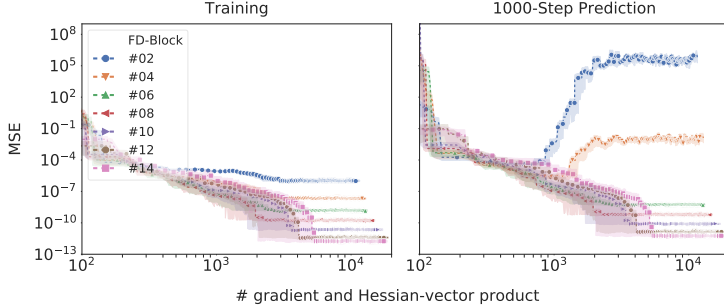
Figure 6: Evolution of the average training & testing errors (and 95% confidence intervals) for different numbers of FD-Blocks & 16 FD-Filters for the unstable case.

As mentioned in Section 3, stacking k FD-Blocks introduces $k - 1$ artificial time steps to the time interval $[t, t + \Delta t]$. While $k = 1$ suffices for the cases with small Δt (i.e., $\Delta t \leq 1$), it is crucial to introduce a sufficient number of artificial time steps in order to achieve good training and testing performance in the setting where Δt is large. Figure 6 shows the results of training the networks with different numbers of FD-Blocks and 16 FD-Filters for the unstable case ($\Delta t = 200$). As is clear, the larger the number of FD-Blocks, the lower the eventual training and testing errors at the cost of training a more complex network.

The size of FD-Net models depend on the number of FD-Filters. Thus far, we illustrated the performance of FD-Net with 16 FD-Filters. Figure 7 shows the results of training the networks with different numbers of FD-Filters and 1 FD-Block on the stable case. The figure clearly shows that the performance of FD-Net with a small number of FD-Filters
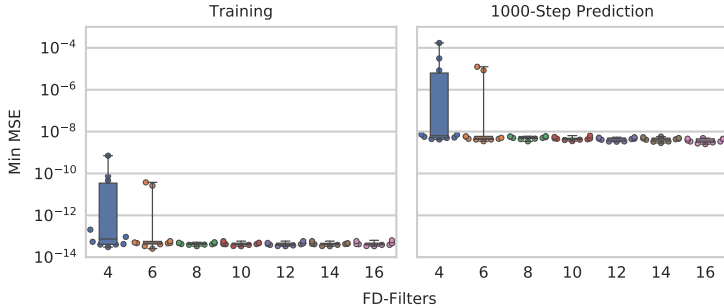
Figure 7: Minimum training & testing errors (with the lower/upper quartiles, medians and ranges) for different numbers of FD-Filters & 1 FD-Block for the stable case.

varies by random seeds, and that utilizing a larger number of FD-Filters reduces this variance. That being said, the results highlight that there is little benefit to using more that 8 FD-Filters, as the average testing error only improves marginally with more FD-Filters. Similar conclusions can be drawn for the other cases; see Appendix B.

5   Final Remarks

In this paper, we presented a novel neural network framework, FD-Net, for learning the dynamics of PDEs and making predictions solely based on trajectory data. The architecture of FD-Net is inspired by finite differences and residual neural networks. FD-Net is able to efficiently learn the dynamics and make predictions for the heat equation in the stable, unstable, forcing and noisy settings. However, this was only a proof-of-concept study of our FD-Net model. As future work, we aim to

study the applicability of `FD-Net` for solving different PDEs (e.g., higher-order, nonlinear, etc) and compare against higher-order and implicit numerical schemes, to extend the territory to discovering hidden PDEs, and to develop customized optimization algorithms for training the networks.

References

[1] Albert S Berahas, Raghu Bollapragada, and Jorge Nocedal. An investigation of newton-sketch and subsampled newton methods. *Optimization Methods and Software*, pages 1–20, 2020.

[2] Albert S Berahas, Majid Jahani, and Martin Takáč. Quasi-newton methods for deep learning: Forget the past, just sample. *arXiv preprint arXiv:1901.09997*, 2019.

[3] Albert S Berahas and Martin Takáč. A robust multi-batch l-bfgs method for machine learning. *Optimization Methods and Software*, 35(1):191–219, 2020.

[4] Josh Bongard and Hod Lipson. Automated reverse engineering of nonlinear dynamical systems. *Proceedings of the National Academy of Sciences*, 104(24):9943–9948, 2007.

[5] Léon Bottou, Frank E Curtis, and Jorge Nocedal. Optimization methods for large-scale machine learning. *Siam Review*, 60(2):223–311, 2018.

[6] Ricky T. Q. Chen, Yulia Rubanova, Jesse Bettencourt, and David K Duvenaud. Neural ordinary differential equations. In *Advances in Neural Information Processing Systems 31*, pages 6571–6583. Curran Associates, Inc., 2018.

[7] Leonhard Euler. *Institutionum calculi integralis*, volume 1. impensis Academiae imperialis scientiarum, 1824.

[8] Amir Barati Farimani, Joseph Gomes, and Vijay S. Pande. Deep learning the physics of transport phenomena. *arXiv preprint arXiv:1709.02432*, 2017.

[9] Kaiming He, Xiangyu Zhang, Shaoqing Ren, and Jian Sun. Deep residual learning for image recognition. In *Proceedings of the IEEE conference on computer vision and pattern recognition*, pages 770–778, 2016.

[10] Frank P Incropera, Adrienne S Lavine, Theodore L Bergman, and David P DeWitt. *Fundamentals of heat and mass transfer*. Wiley, 2007.

[11] Diederik P. Kingma and Jimmy Ba. Adam: A method for stochastic optimization. *arXiv preprint arXiv:1412.6980*, 2014.

[12] Zichao Long, Yiping Lu, and Bin Dong. Pde-net 2.0: Learning pdes from data with a numeric-symbolic hybrid deep network. *Journal of Computational Physics*, 399:108925, 2019.

[13] Zichao Long, Yiping Lu, Xianzhong Ma, and Bin Dong. PDE-net: Learning PDEs from data. In *Proceedings of the 35th International Conference on Machine Learning*, volume 80 of *Proceedings of Machine Learning Research*, pages 3208–3216, Stockholmsmässan, Stockholm Sweden, 10–15 Jul 2018. PMLR.

[14] Jorge Nocedal and Stephen J. Wright. *Numerical Optimization*. Springer-Verlag New York, 2 edition, 2006.

[15] Louise Olsen-Kettle. Numerical solution of partial differential equations. *Lecture notes at University of Queensland, Australia*, 2011.

[16] Maziar Raissi and George Em Karniadakis. Hidden physics models: Machine learning of nonlinear partial differential equations. *Journal of Computational Physics*, 357:125–141, 2018.

[17] Maziar Raissi, Paris Perdikaris, and George Em Karniadakis. Physics informed deep learning (part ii): Data-driven discovery of nonlinear partial differential equations. *arXiv preprint arXiv:1711.10566*, 2017.

[18] Farbod Roosta-Khorasani and Michael W. Mahoney. Sub-sampled newton methods. *Mathematical Programming*, 174(1):293–326, 2019.

[19] Samuel H Rudy, Steven L Brunton, Joshua L Proctor, and J Nathan Kutz. Data-driven discovery of partial differential equations. *Science Advances*, 3(4):e1602614, 2017.

[20] Hayden Schaeffer. Learning partial differential equations via data discovery and sparse optimization. *Proceedings of the Royal Society A: Mathematical, Physical and Engineering Sciences*, 473(2197):20160446, 2017.

[21] Michael Schmidt and Hod Lipson. Distilling free-form natural laws from experimental data. *Science*, 324(5923):81–85, 2009.

[22] Trond Steihaug. The conjugate gradient method and trust regions in large scale optimization. *SIAM Journal on Numerical Analysis*, 20(3):626–637, 1983.

[23] Peng Xu, Fred Roosta, and Michael W Mahoney. Second-order optimization for non-convex machine learning: An empirical study. In *Proceedings of the 2020 SIAM International Conference on Data Mining*, pages 199–207. SIAM, 2020.

A Exact solutions to PDEs

In this section, we derive the exact solutions to the PDEs we investigate. Although these results are well-known, we state them here for completeness.

A.1 No Forcing

Given the heat equation (2) defined on a 1-D bar of length L with a rate of diffusion β, the boundary conditions (3) and the initial condition (4), we restate the exact solution (5) in the following

$$u(x, t) = \sum_{i=1}^{N} C_i \sin\left(\frac{i\pi x}{L}\right) e^{-\beta(i\pi/L)^2 t}.$$

A.2 With Forcing

Given the forcing function and the corresponding equation (7), the exact solution is

$$u(x, t) = \sum_{i=1}^{N} \left(C_i - \frac{D_i}{\beta(i\pi/L)^2}\right) \sin\left(\frac{i\pi x}{L}\right) e^{-\beta(i\pi/L)^2 t} + \sum_{i=1}^{N} \frac{D_i}{\beta(i\pi/L)^2} \sin\left(\frac{i\pi x}{L}\right). \quad (10)$$

B Extended Numerical Results

B.1 Detailed Description of Experiments

In this section, we describe the approach and implementation of the experiments in detail.

B.1.1 Data Generation

Following the descriptions in Section 4.1, the 200 ICs were generated randomly with 200 distinct random seeds. We generated the data set of the solution (5) for the stable case and used it as our base data for the noisy and unstable cases. Specifically, the noisy data set was formed by adding the multiplicative noises to the base data; the unstable data set was formed by extracting the data of $t \in \{0, 200, 400, 600, 800, 1000\}$ from the base data. For the forcing case, we used a randomly generated forcing function to create the data set of solution (10).

B.1.2 Supplementary Testing Procedures

In addition to the 1000-step prediction studied in Section 4, we adopted two supplementary testing procedures, i.e., the one-step and multi-step predictions, to evaluate the networks' performance of making short-term predictions.

Given a Δt, let $\tau' \in \mathbb{N}^+$ s.t. $\tau' \Delta t \leq T$ and consider a generalized testing data set

$$A_{\text{test}_{\tau'}} = \left\{(u_s(x, t), u_s(x, t + \tau' \Delta t)) \mid s \in S_{\text{test}},\ x \in \{0, \Delta x, ..., L\},\ t \in \{0, \Delta t, ..., T - \tau' \Delta t\}\right\},$$

where S_{test} is the index set of ICs for the testing purposes, $(u_s(x, t), u_s(x, t + \tau' \Delta t))$ is a testing sample, $u_s(x, t)$ is the input to the network, and $u_s(x, t + \tau' \Delta t)$ is the target.

The one-step prediction procedure is consistent with the training procedure, and we used $\tau' = 1$ for all cases. To define the multi-step prediction, we let $\tau' = 10$ for the stable, noisy and forcing cases and $\tau' = 3$ for the unstable case. (Note that when $\tau' = 5$ for the unstable case or $\tau' = 1000$ for one of the others, we have the data set for the 1000-step prediction.)

Accordingly, we defined the testing error as MSE in a generalized form

$$\text{MSE}_{\text{test}_{\tau'}} = \frac{1}{|A_{\tau'}|} \sum_{s,x,t} \left(u_s(x, t + \tau' \Delta t) - \tilde{u}_s(x, t + \tau' \Delta t)\right)^2, \quad (11)$$

where $\tilde{u}_s(x, t + \tau' \Delta t)$ denotes a prediction made by the network.

B.1.3 Implementation and Design of Experiments

We implemented the networks in Python with PyTorch and trained the networks on an *NVIDIA K80* GPU. For the optimization methods, we implemented the Trust-Region (TR) Newton CG method in Python and used the ADAM optimizer of PyTorch.

The primary goal of the experiments conducted in this paper is to evaluate the training and testing performance of the networks. To this end, we chose different configurations (see Table 2) and adopted three testing procedures for each case. And, for each configuration, we trained the network with the TR methods and ADAM with learning rates 10^{-3} and 10^{-4}, and used 10 distinct random seeds to initialize the network parameters and to select the stochastic mini-batches. We constrained the training budget of TR to be 100 iterations for the stable, noisy and forcing cases and 300 iterations for the unstable case. And, we allowed the ADAM algorithms to run for 12000 iterations regardless of a case.

Table 2: Network Configurations.

Hyper-Parameter	Unstable Case	Others[†]
# FD-Blocks	$1, 2, 3, 4, 6, 8, 10$	$1, 2, 3, 4$
# FD-Filters	$2, 4, 8, 16$	$2, 4, 8, 16$

[†] includes the stable, noisy and forcing cases.

To study the effects of the hyper-parameters, i.e., the number of FD-Blocks and FD-Filters, and to validate our design of the architecture, we conducted further experiments with different numbers of FD-Blocks against the unstable case and with different numbers of FD-Filters against the stable case.

In the following sections, we will present the full experimental results in the order of the stable case, the unstable case, the forcing case and the noisy case.

B.2 Stable Case

In this section, we present the experimental results of the stable case. Figure 8 shows the evolution of the training errors of different configurations. Figure 9 shows the sequential predictions and the squared errors, and Figure 10 shows the minimum testing errors (over the training process) of the 1000-step predictions by configuration. In addition, Figure 11 shows the relationship between the training and testing errors (note: the lower and to the left is better). For the two supplementary testing procedures described in Section B.1.2, given the data of solution at t, the one-step prediction is made at $t + \Delta t$, i.e., $t + 1$, and the multi-step prediction is made at $t + 10\Delta t$, i.e., $t + 10$. Figures 12 & 13 show the evolutions of the testing errors (11) and Figures 14 & 15 show the minimum testing errors of the one- and multi-step predictions. To summarize the testing performance, we put the minimum testing errors aggregated over all configurations in Figure 16. Besides, the results of the sensitivity analysis on different numbers of FD-Filters (and 1 FD-Block) are shown in Figure 17, which shows the evolution and the minimum (over the training process) of the training and testing errors.
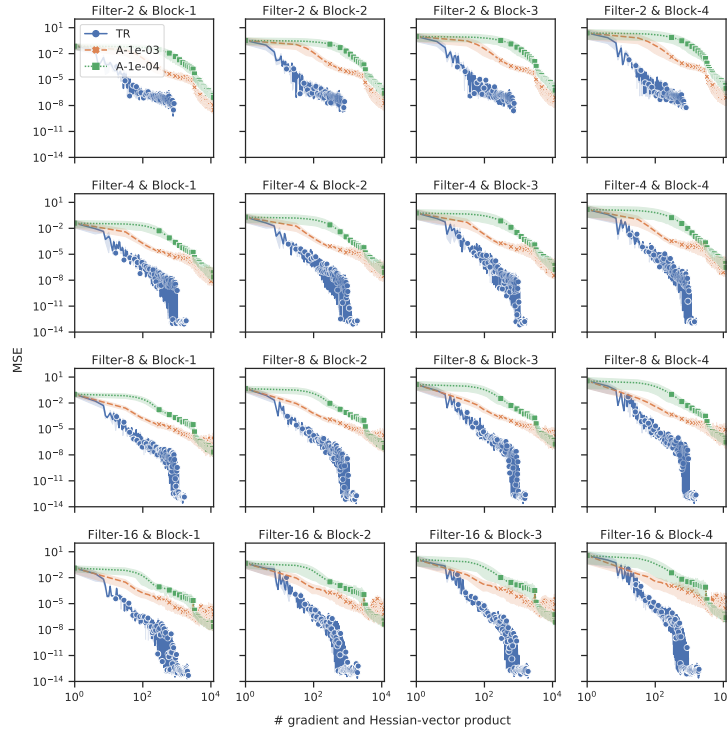
Figure 8: **Stable Case:** Evolution of the MSE loss of stochastic mini-batch by configuration.
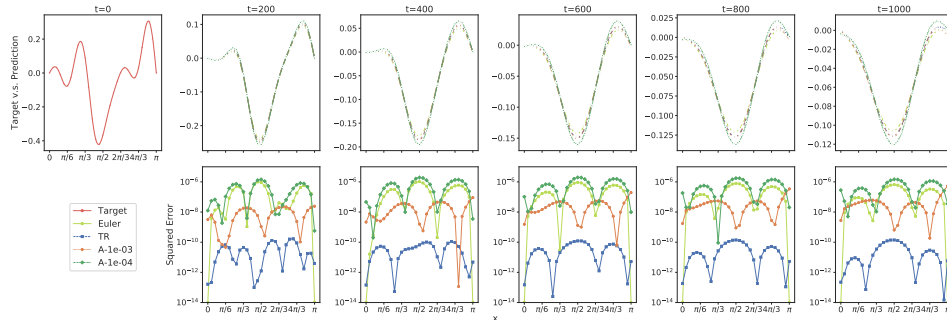
Figure 9: **Stable Case:** Sequence of predictions.

13
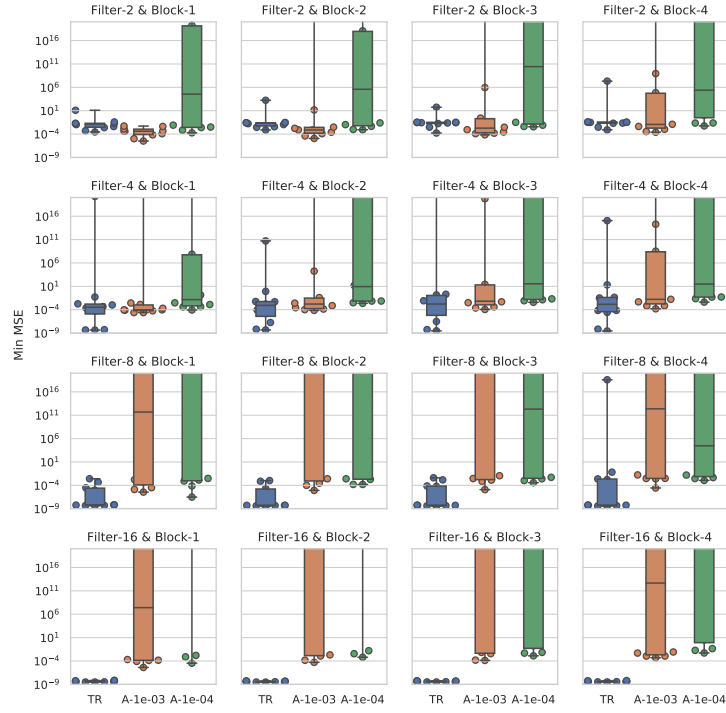
Figure 10: **Stable Case:** Minimum testing errors by configuration - 1000-step prediction.
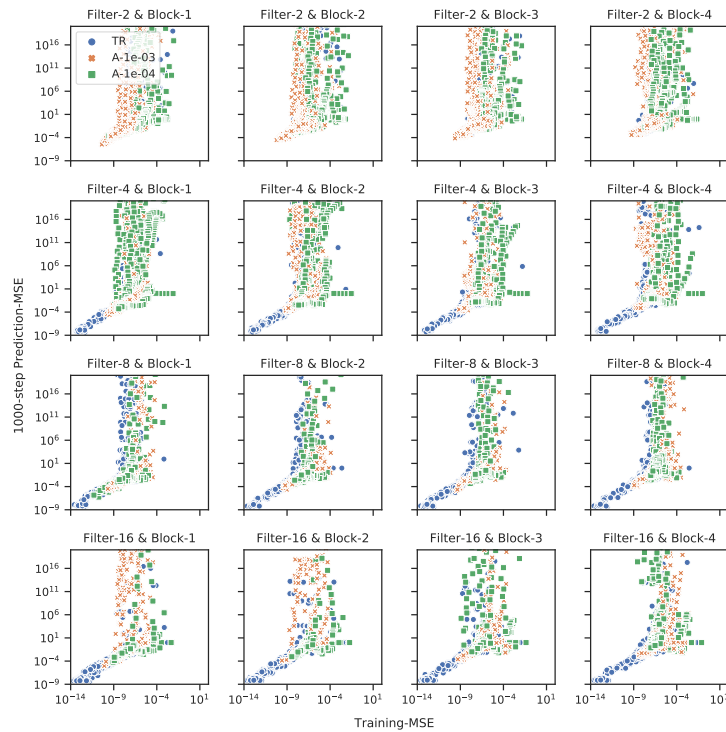
Figure 11: **Stable Case:** Training vs. 1000-step prediction errors (over the training process) by configuration.
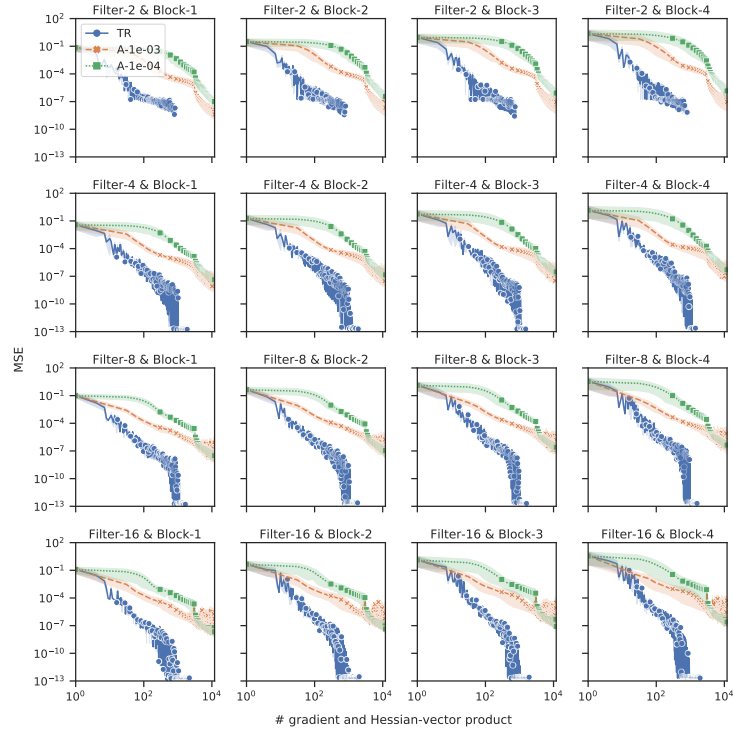
Figure 12: **Stable Case:** Evolution of the testing errors by configuration - one-step prediction.
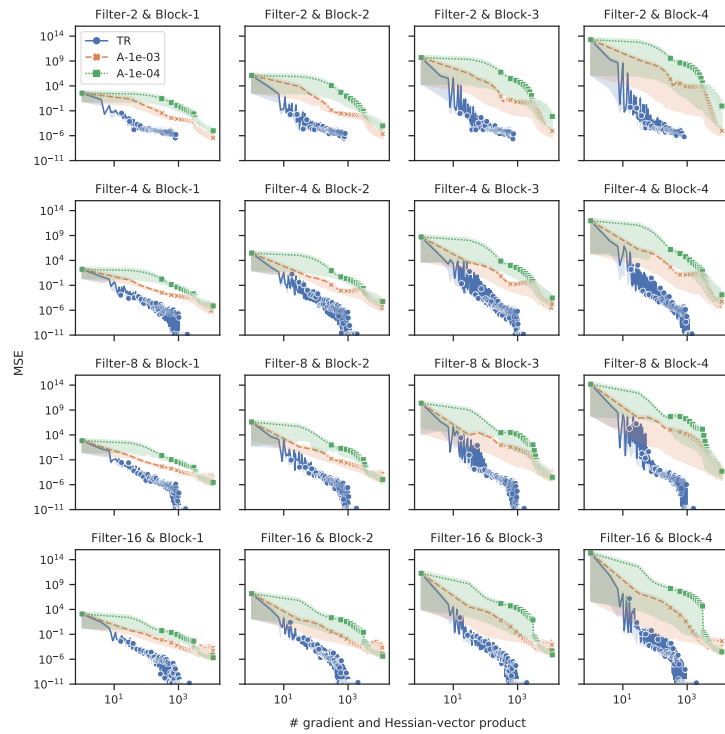
Figure 13: **Stable Case:** Evolution of the testing errors by configuration - multi-step prediction.
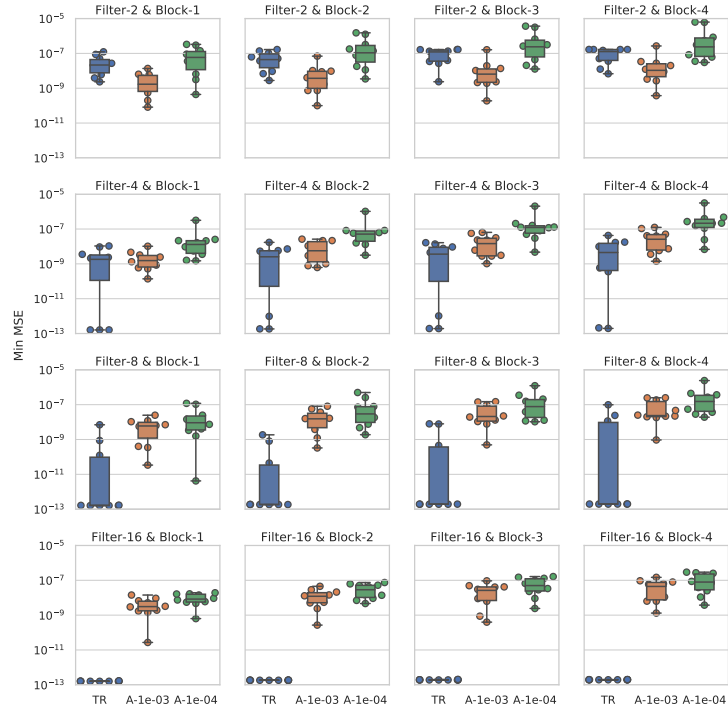
Figure 14: **Stable Case:** Minimum testing errors by configuration - one-step prediction.
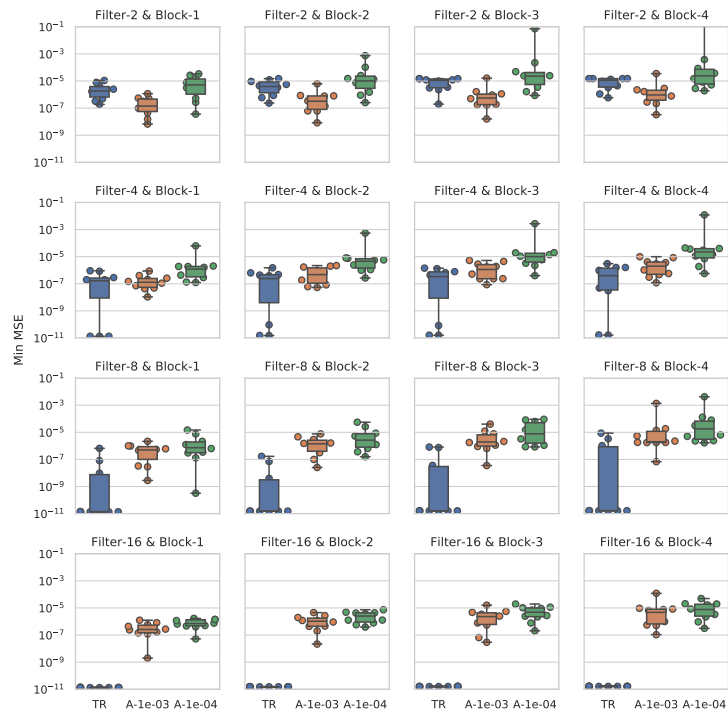
Figure 15: **Stable Case:** Minimum testing errors by configuration - multi-step prediction.
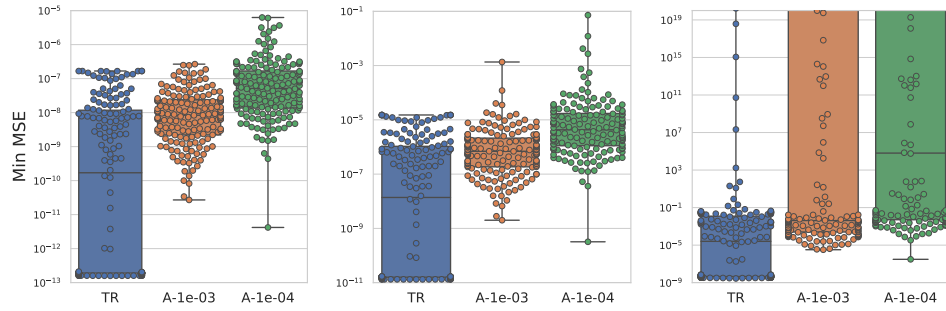
Figure 16: **Stable Case:** The minimum testing errors of the one-step (left), multi-step (middle) and 1000-step (right) predictions (aggregated over all configurations).
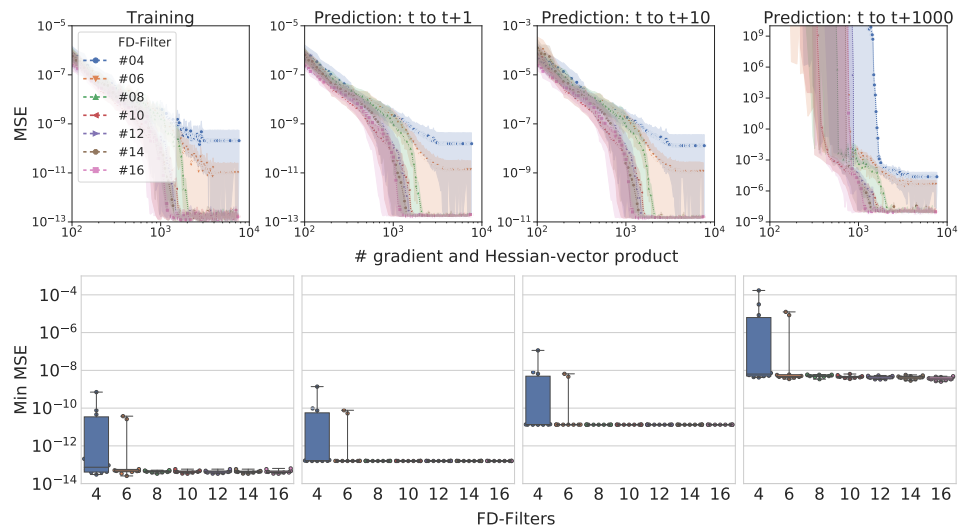
Figure 17: **Stable Case:** The evolution (first row) and the minimum (second row) of the training errors and testing errors of the one-, multi- and 1000-step predictions by configuration of `FD-Filters`.

B.3 Unstable Case

In this section, we present the experimental results of the unstable case. Figure 18 shows the evolution of the training errors of different configurations. Figure 19 shows the sequential predictions and the squared errors, and Figure 20 shows the minimum testing errors (over the training process) of the 1000-step predictions by configuration. In addition, Figure 21 shows the relationship between the training and testing errors (note: the lower and to the left is better). For the two supplementary testing procedures described in Section B.1.2, given the data of solution at t, the one-step prediction is made at $t + \Delta t$, i.e., $t + 200$, and the multi-step prediction is made at $t + 3\Delta t$, i.e., $t + 600$. Figures 22 & 23 show the evolutions of the testing errors (11) and Figures 24 & 25 show the minimum testing errors of the one- and multi-step predictions. To summarize the testing performance, we put the minimum testing errors aggregated over all configurations in Figure 26. Besides, the results of the sensitivity analysis on different numbers of FD-Blocks (and 16 FD-Filters) are shown in Figure 27, which shows the evolution and the minimum (over the training process) of the training and testing errors.
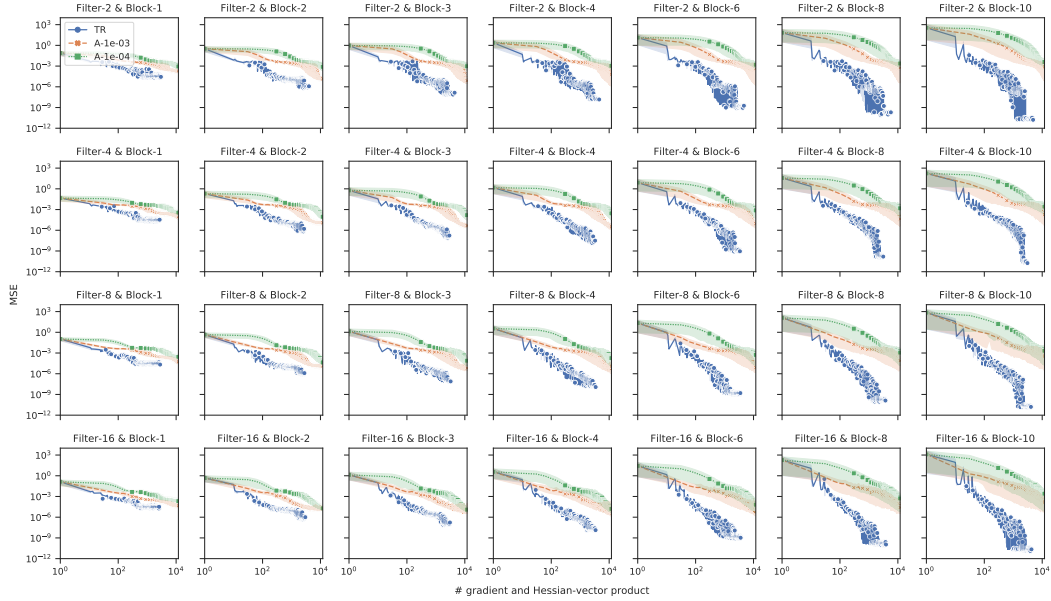
Figure 18: **Unstable Case:** Evolution of the MSE loss of stochastic mini-batch by configuration.
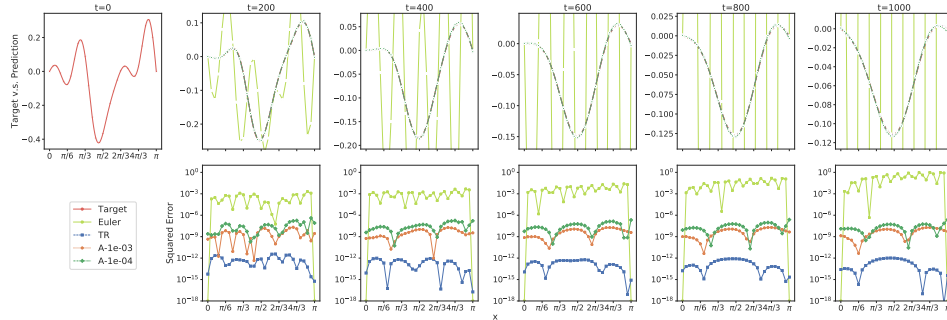
Figure 19: **Unstable Case:** Sequence of predictions.
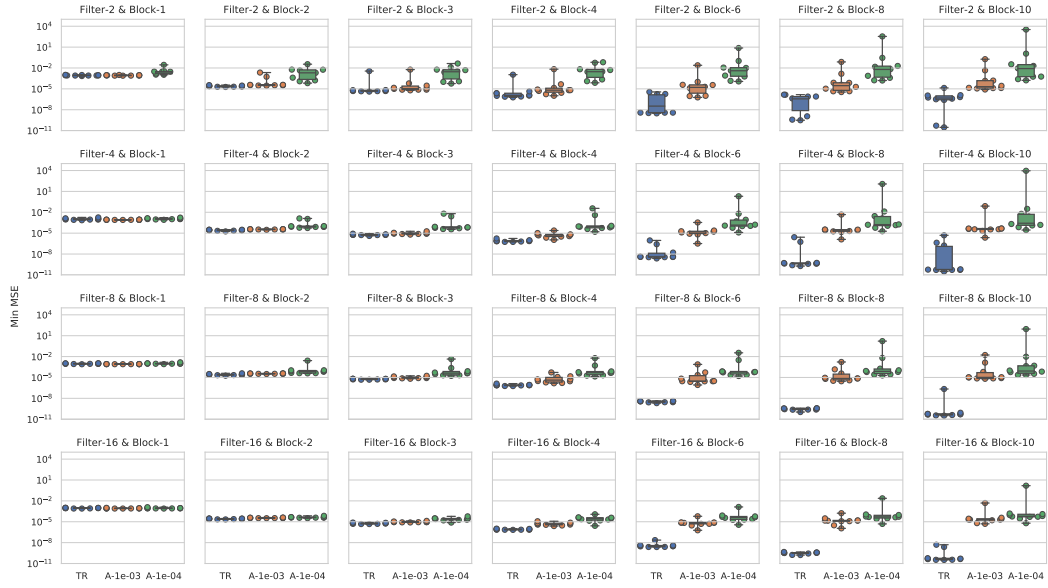
Figure 20: **Unstable Case:** Minimum testing errors by configuration - 1000-step prediction.
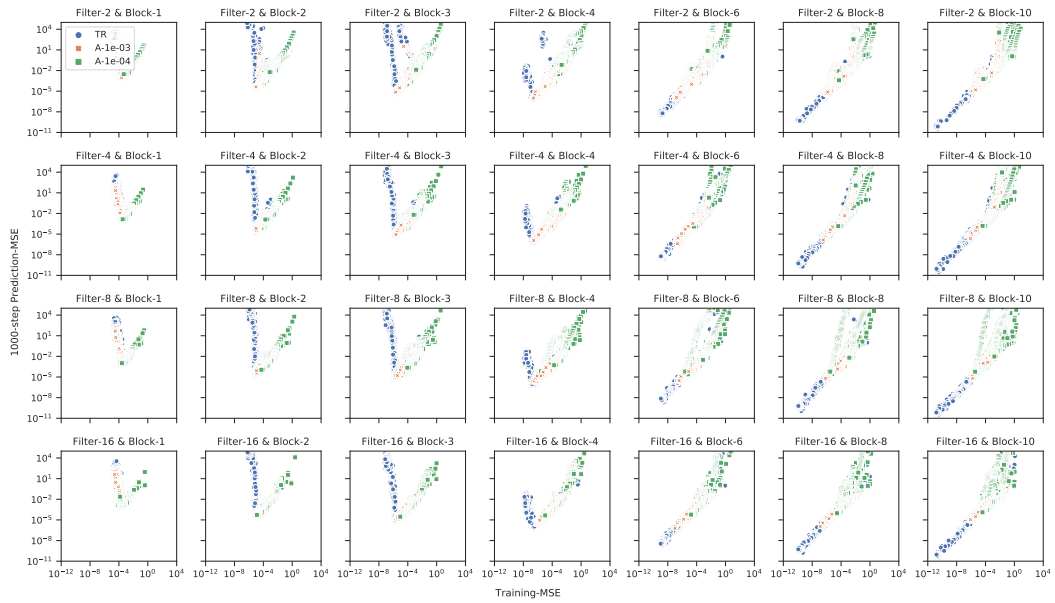
Figure 21: **Unstable Case:** Training vs. 1000-step prediction errors (over the training process) by configuration.
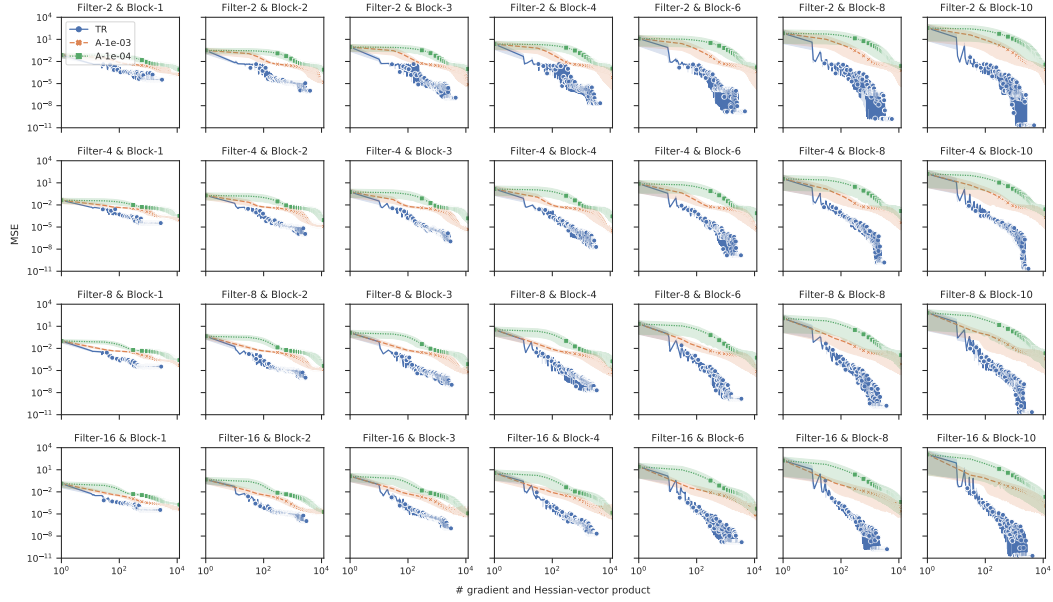
Figure 22: **Unstable Case:** Evolution of the testing errors by configuration - one-step prediction.
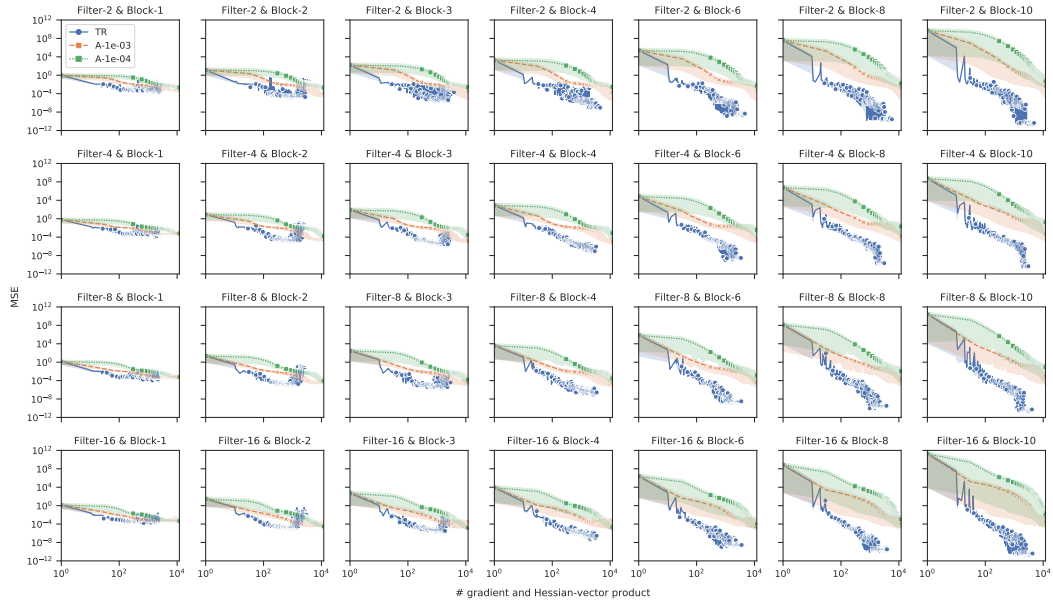
Figure 23: **Unstable Case:** Evolution of the testing errors by configuration - multi-step prediction.
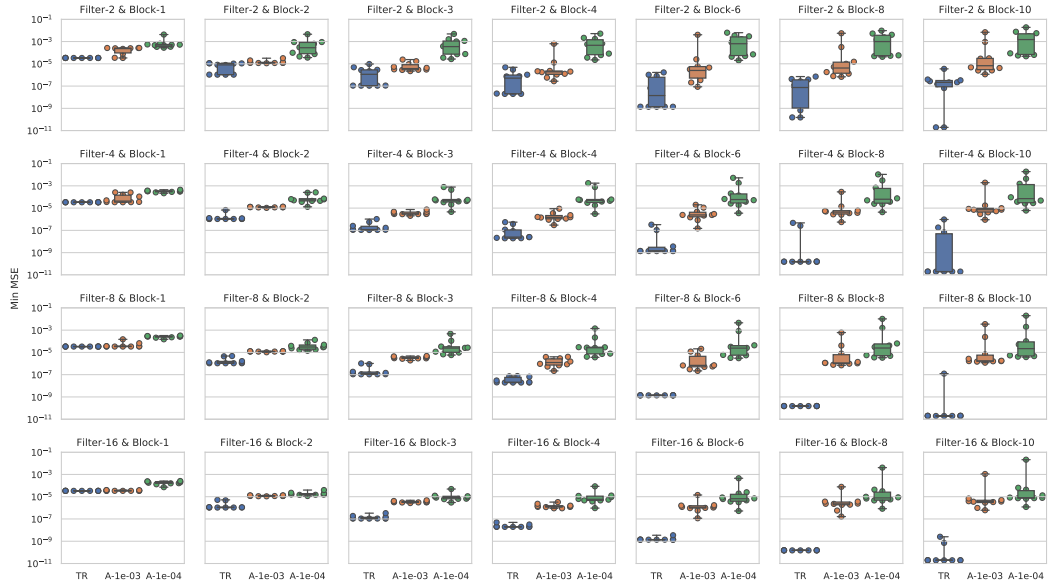
Figure 24: **Unstable Case:** Minimum testing errors by configuration - one-step prediction.

Figure 25: **Unstable Case:** Minimum testing errors by configuration - multi-step prediction.
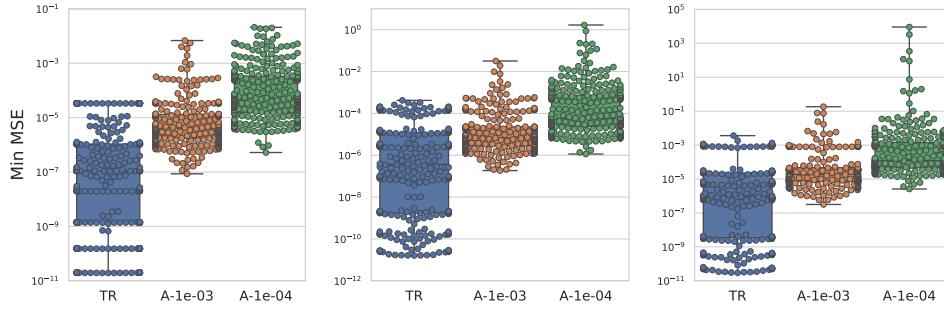
Figure 26: **Unstable Case:** The minimum testing errors of the one-step (left), multi-step (middle) and 1000-step (right) predictions (aggregated over all configurations).
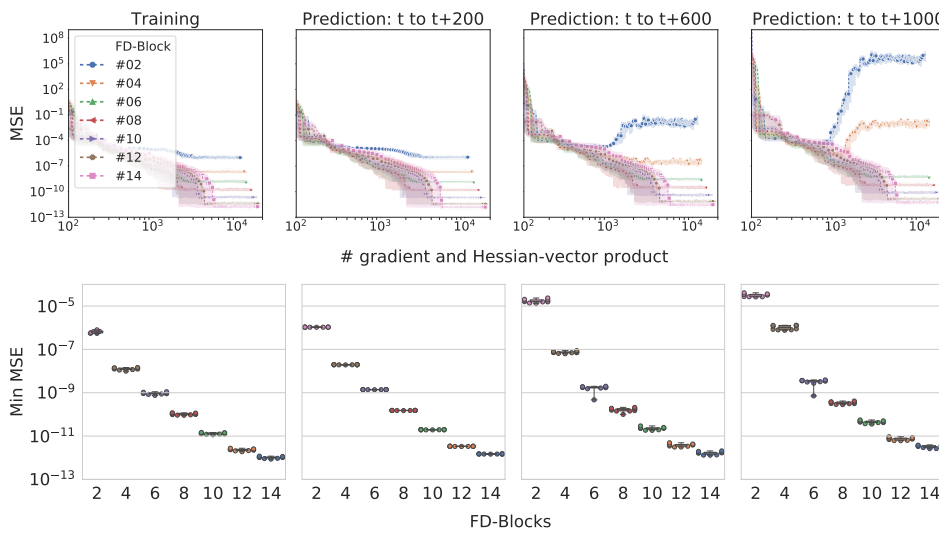
Figure 27: **Unstable Case:** The evolution (first row) and the minimum (second row) of the training errors and testing errors of the one-, multi- and 1000-step prediction by configuration of `FD-Blocks`.

B.4 Forcing Case

In this section, we present the experimental results of the forcing case. Figure 28 shows the evolution of the training errors of different configurations. Figure 29 shows the sequential predictions and the squared errors, and Figure 30 shows the minimum testing errors (over the training process) of the 1000-step predictions by configuration. In addition, Figure 31 shows the relationship between the training and testing errors (note: the lower and to the left is better). For the two supplementary testing procedures described in Section B.1.2, given the data of solution at t, the one-step prediction is made at $t + \Delta t$, i.e., $t + 1$, and the multi-step prediction is made at $t + 10\Delta t$, i.e., $t + 10$. Figures 32 & 33 show the evolutions of the testing errors (11) and Figures 34 & 35 show the minimum testing errors of the one- and multi-step predictions. To summarize the testing performance, we put the minimum testing errors aggregated over all configurations in Figure 36.
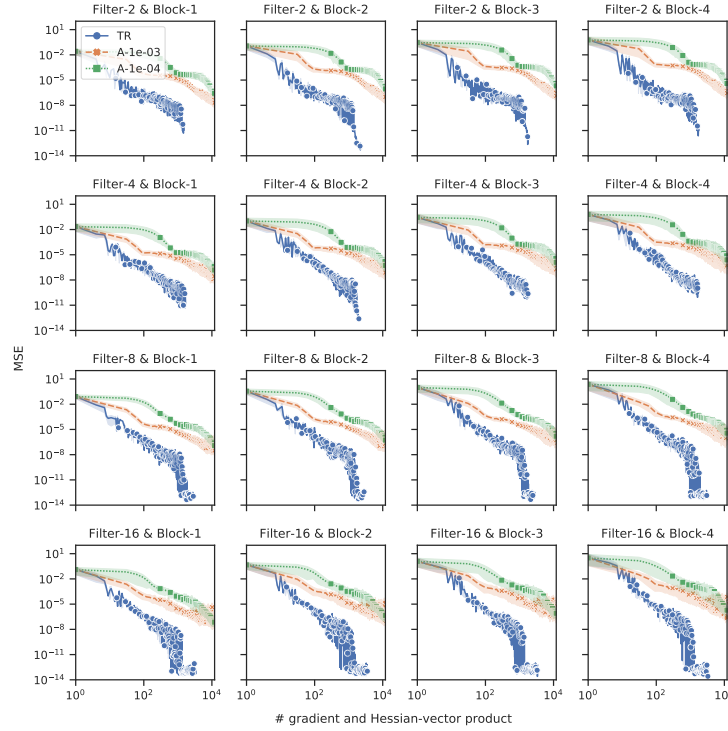
Figure 28: **Forcing Case:** Evolution of the MSE loss of stochastic mini-batch by configuration.
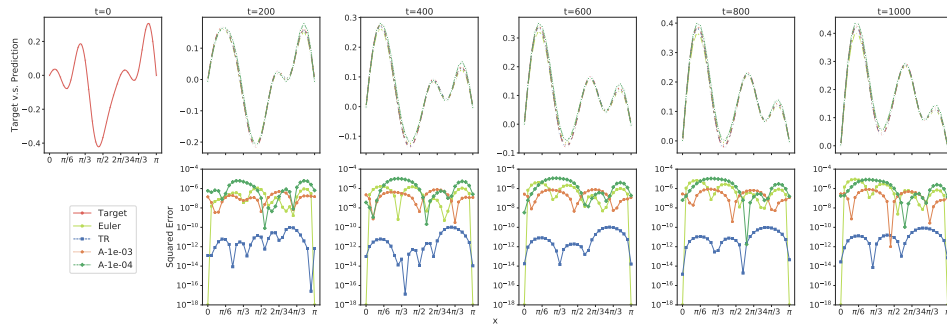
Figure 29: **Forcing Case:** Sequence of predictions.
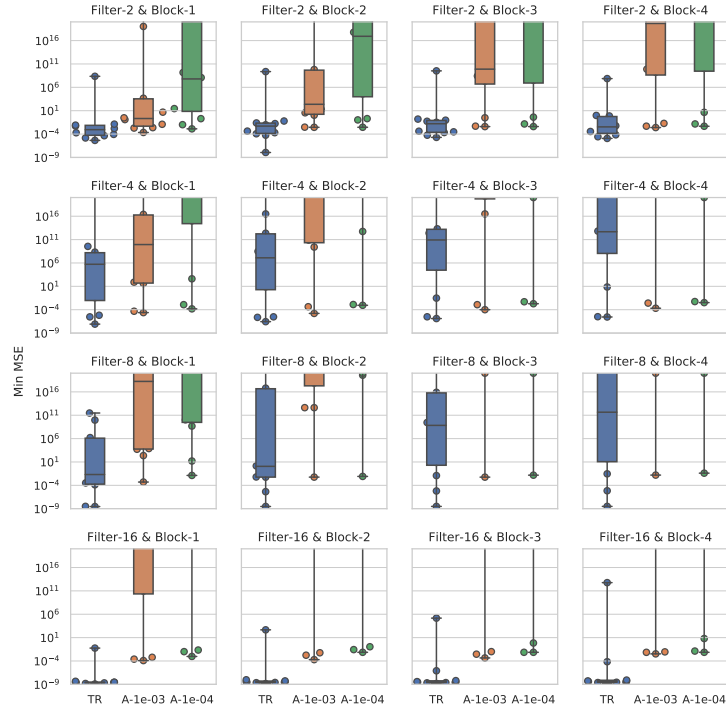
Figure 30: **Forcing Case:** Minimum testing errors by configuration - 1000-step prediction.
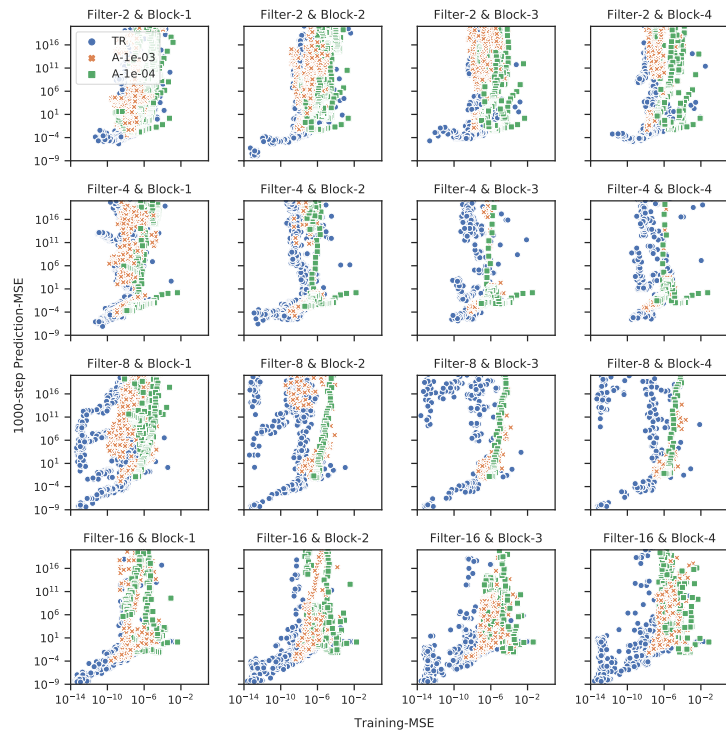
Figure 31: **Forcing Case:** Training vs. 1000-step prediction errors (over the training process) by configuration.
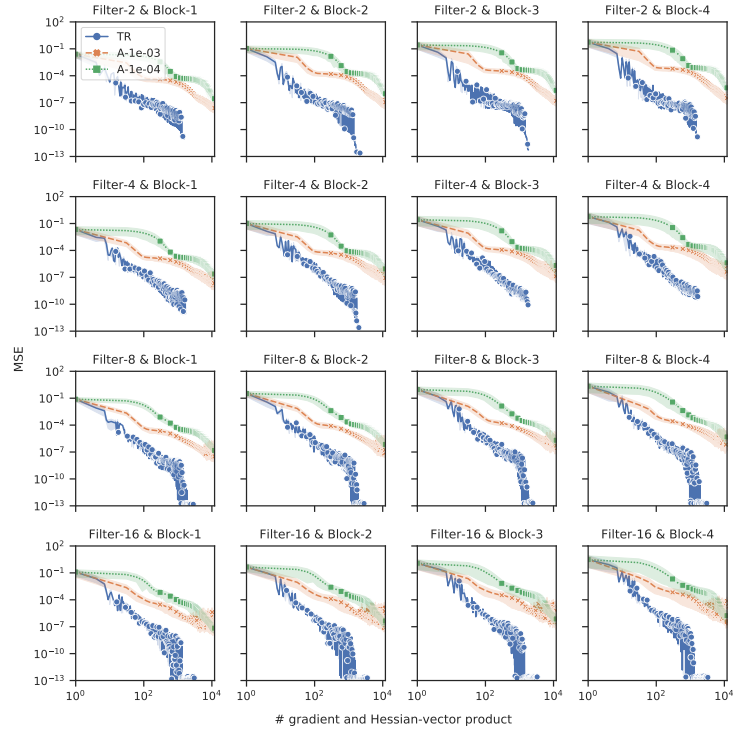
Figure 32: **Forcing Case:** Evolution of the testing errors by configuration - one-step prediction.
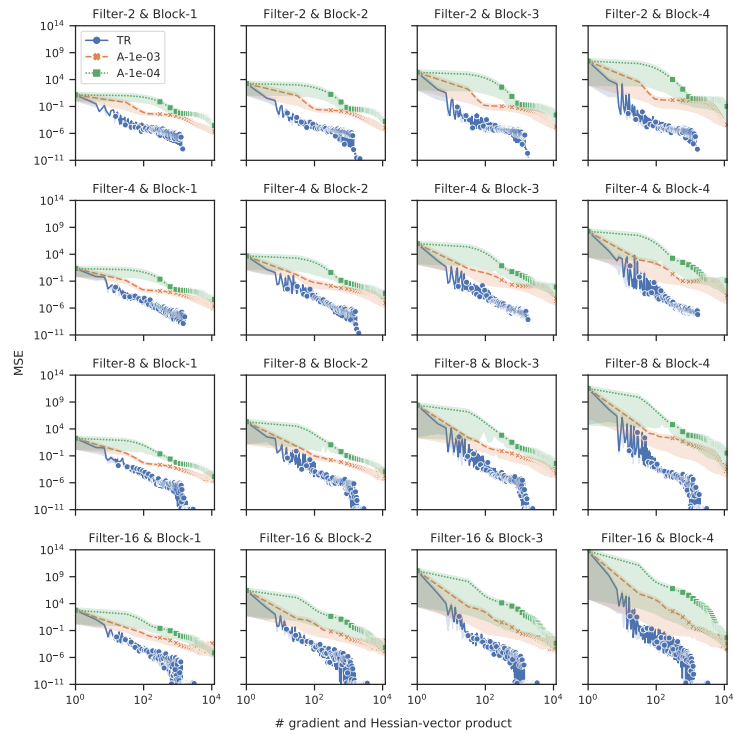
Figure 33: **Forcing Case:** Evolution of the testing errors by configuration - multi-step prediction.
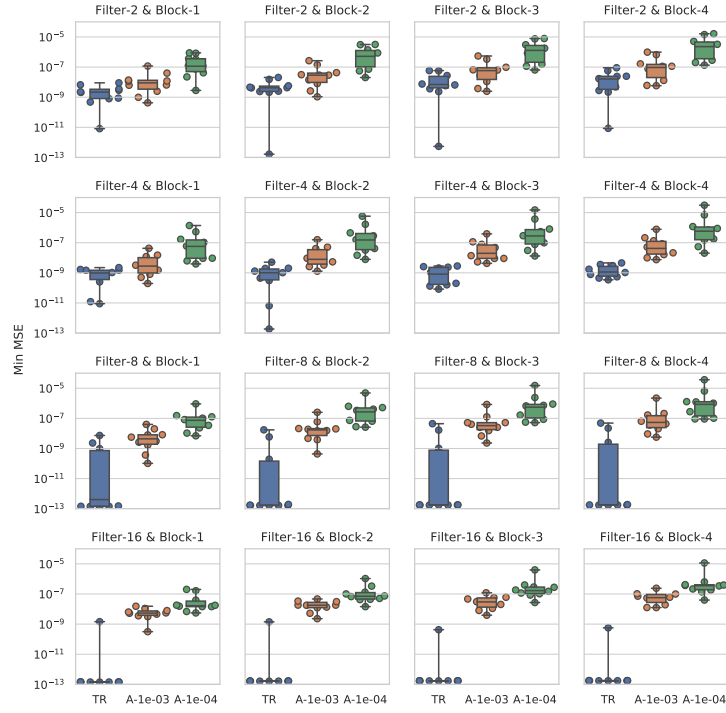
Figure 34: **Forcing Case:** Minimum testing errors by configuration - one-step prediction.
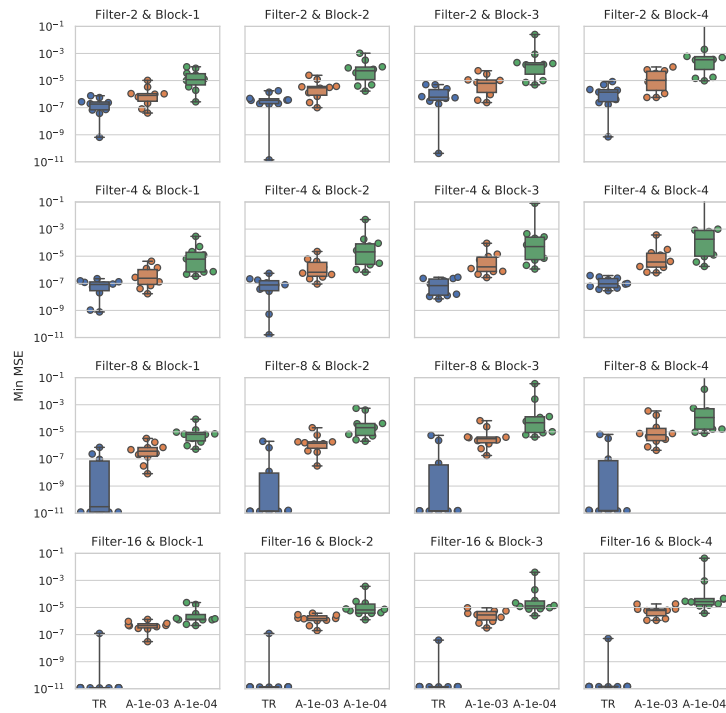
Figure 35: **Forcing Case:** Minimum testing errors by configuration - multi-step prediction.
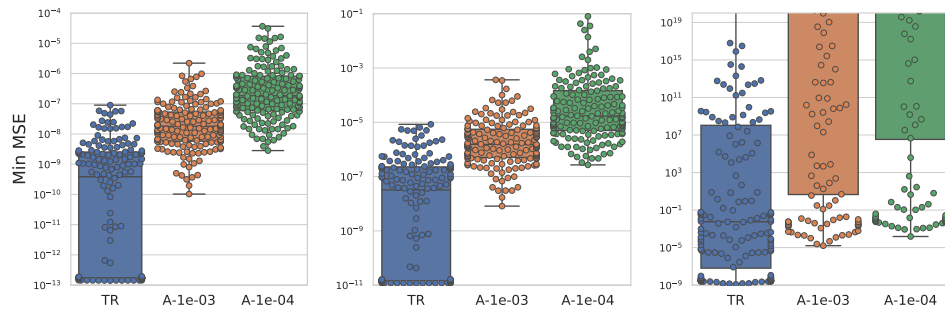
Figure 36: **Forcing Case:** The minimum testing errors of the one-step (left), multi-step (middle) and 1000-step (right) predictions (aggregated over all configurations).

B.5 Noisy Case

In this section, we present the experimental results of the noisy case. Figure 37 shows the evolution of the training errors of different configurations. Figure 38 shows the sequential predictions and the squared errors, and Figure 39 shows the minimum testing errors (over the training process) of the 1000-step predictions by configuration. In addition, Figure 40 shows the relationship between the training and testing errors (note: the lower and to the left is better). For the two supplementary testing procedures described in Section B.1.2, given the data of solution at t, the one-step prediction is made at $t + \Delta t$, i.e., $t + 1$, and the multi-step prediction is made at $t + 10\Delta t$, i.e., $t + 10$. Figures 41 & 42 show the evolutions of the testing errors (11) and Figures 43 & 44 show the minimum testing errors of the one- and multi-step predictions. To summarize the testing performance, we put the minimum testing errors aggregated over all configurations in Figure 45.

We further conducted experiments on the sensitivity of FD-Net to 10 different levels of the multiplicative noise and used 1 FD-Block and 16 FD-Filters to configure the networks. Figure 46 shows the evolution of the training errors, Figure 47 show the minimum testing errors over the training process, and Figure 48 shows the relationship between the training and testing errors in the training process.

(a) Low Noise

(b) Medium Noise
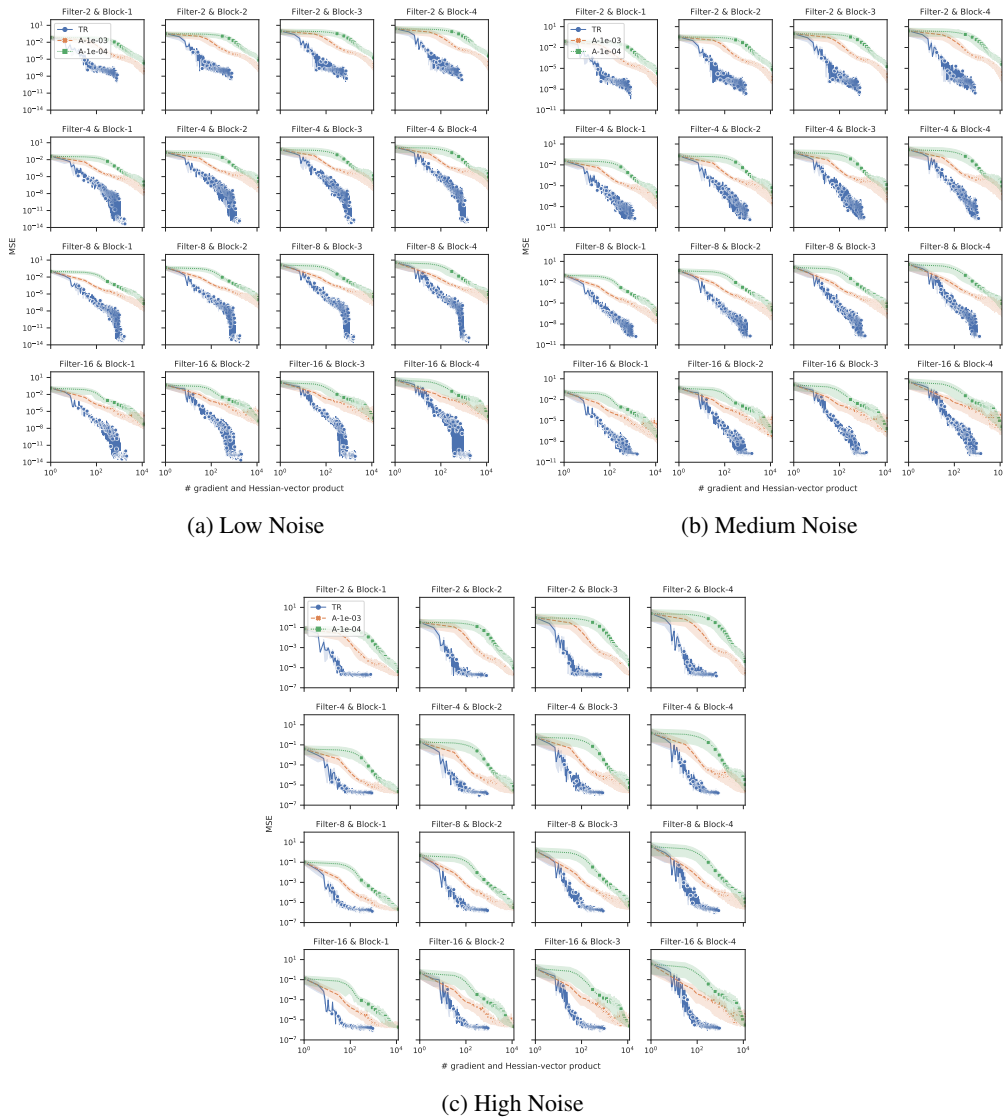
(c) High Noise

Figure 37: **Noisy Case:** Evolution of the MSE loss of stochastic mini-batch by level of noise and configuration.
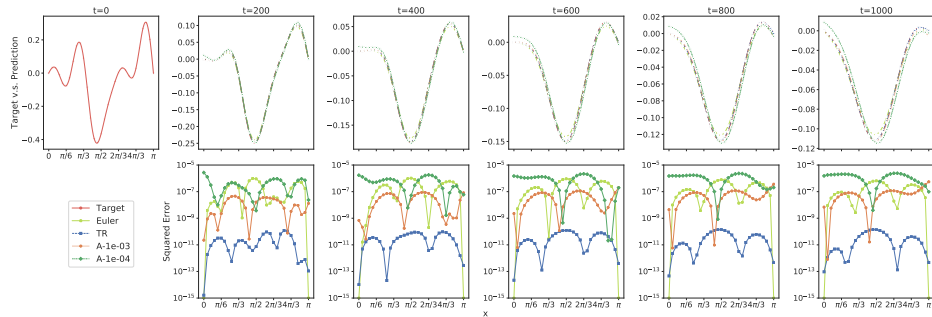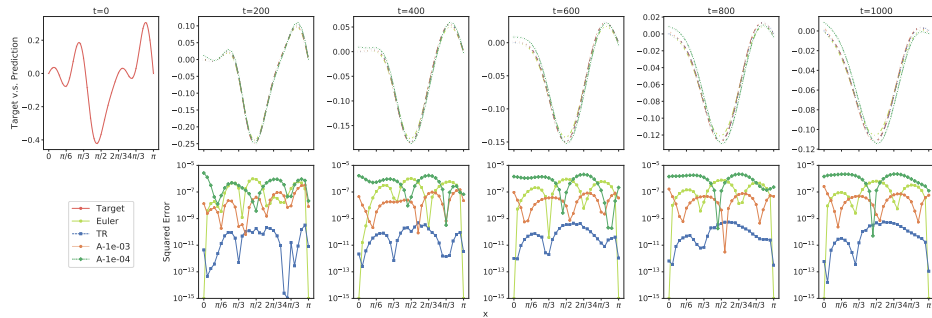
(a) Low Noise
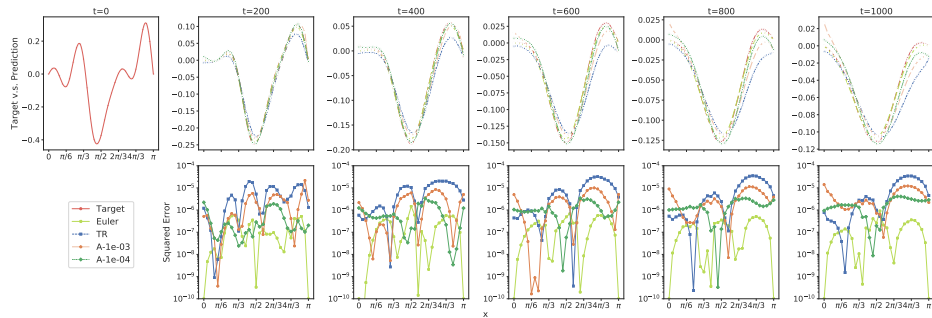
(b) Medium Noise

(c) High Noise

Figure 38: **Noisy Case:** Sequence of predictions by level of noise.

(a) Low Noise

(b) Medium Noise
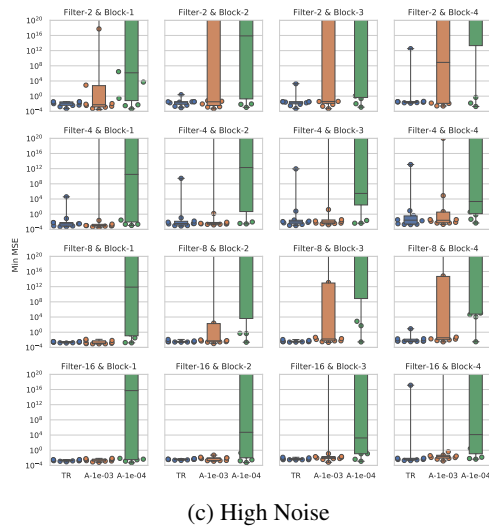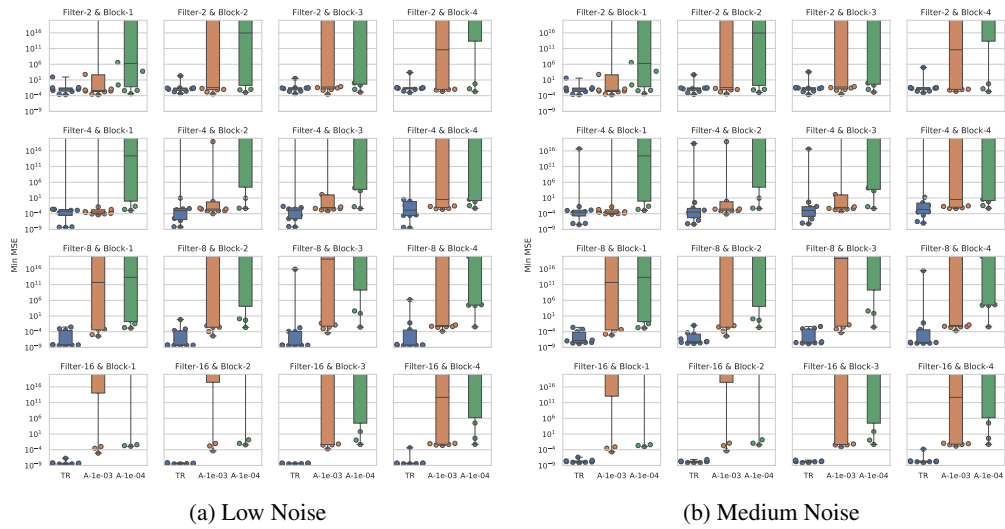
(c) High Noise

Figure 39: **Noisy Case:** Minimum testing errors by level of noise and configuration - 1000-step prediction.
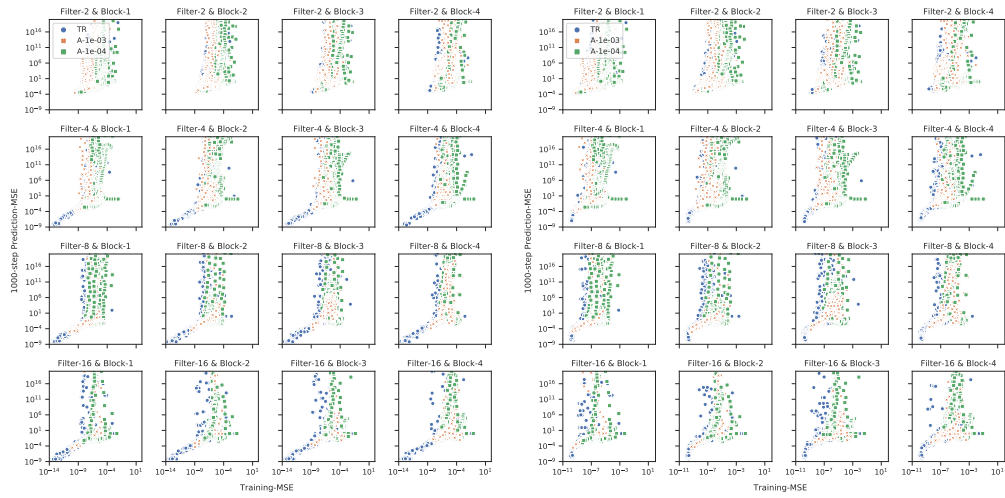
(a) Low Noise
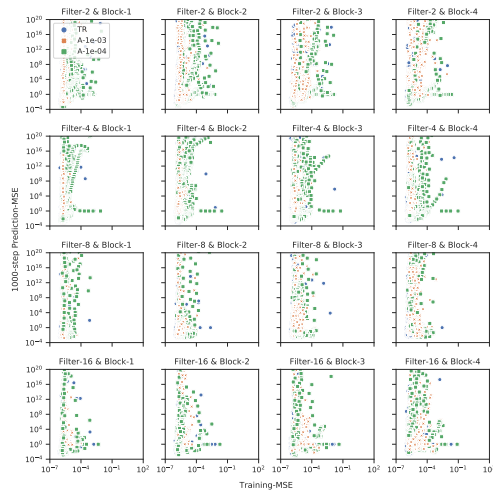
(b) Medium Noise

(c) High Noise

Figure 40: **Noisy Case:** Training vs. 1000-step prediction errors (over the training process) by level of noise and configuration.
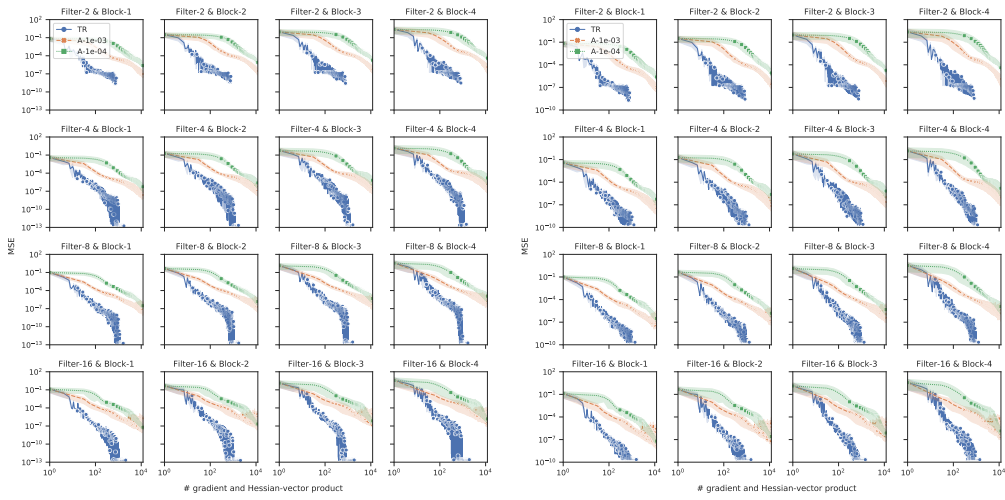
(a) Low Noise
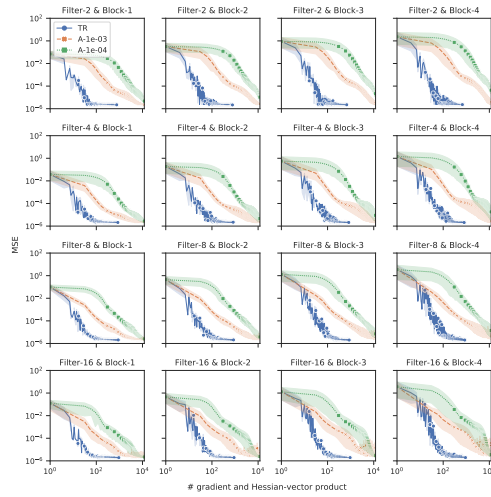
(b) Medium Noise

(c) High Noise

Figure 41: **Noisy Case:** Evolution of the testing errors by level of noise and configuration - one-step prediction.
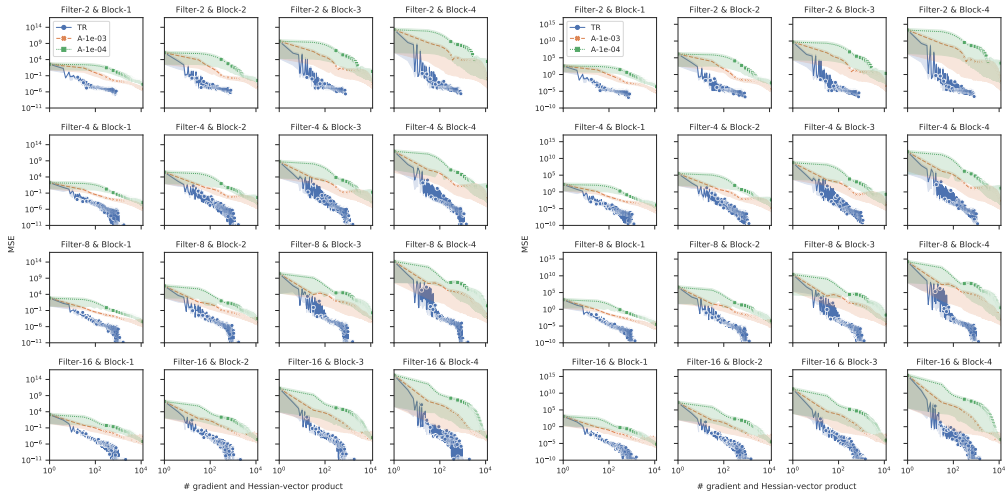
(a) Low Noise
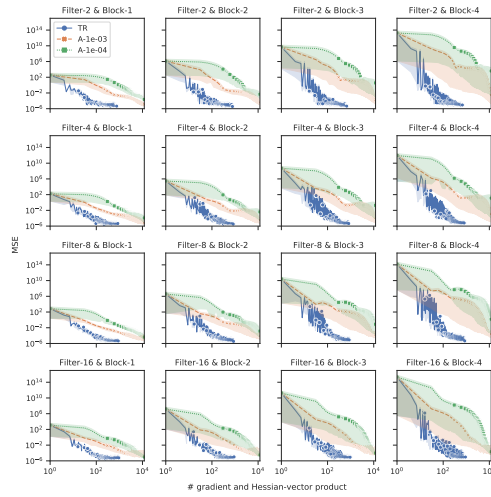
(b) Medium Noise

(c) High Noise

Figure 42: **Noisy Case:** Evolution of the testing errors by level of noise and configuration - multi-step prediction.
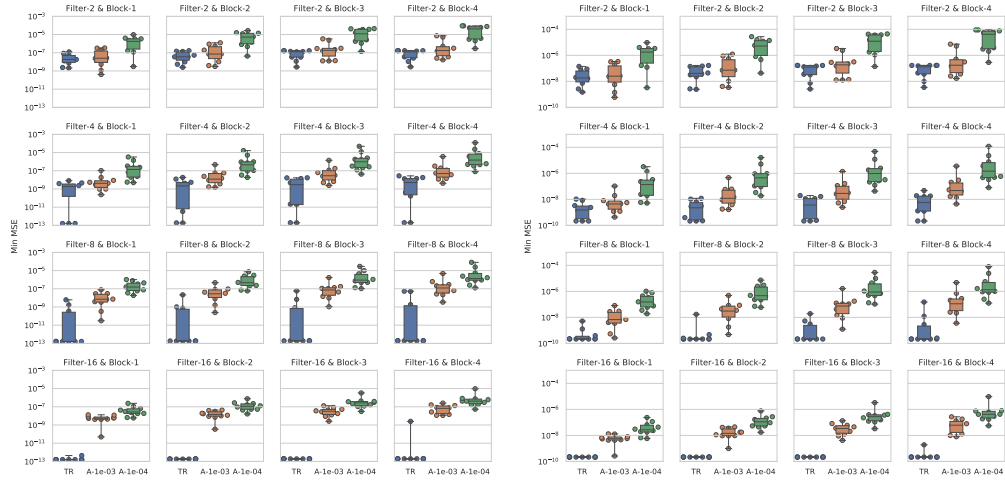
(a) Low Noise
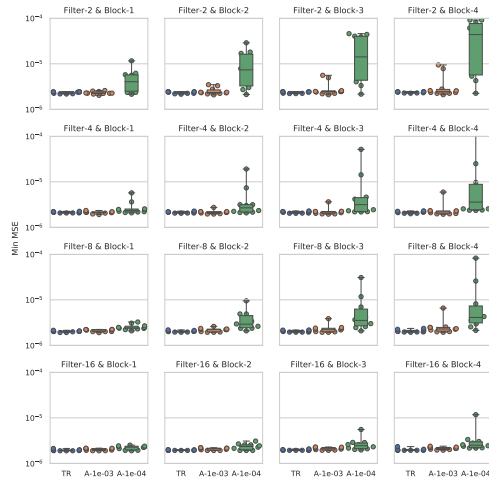
(b) Medium Noise

(c) High Noise

Figure 43: **Noisy Case:** Minimum testing errors by level of noise and configuration - one-step prediction.
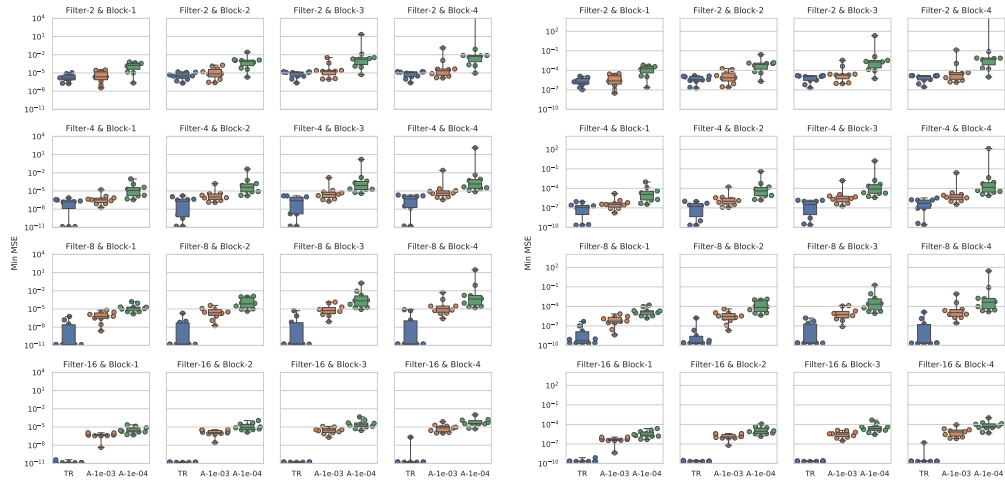
(a) Low Noise

(b) Medium Noise
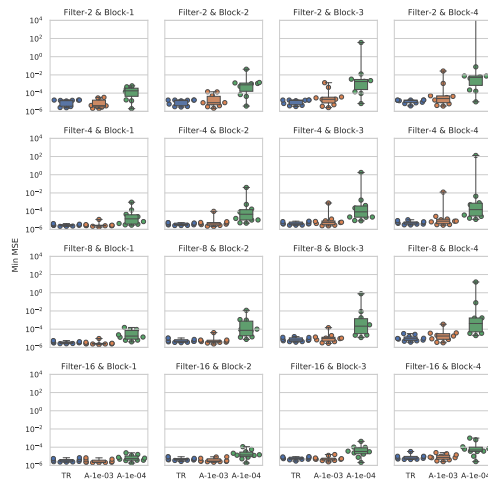
(c) High Noise

Figure 44: **Noisy Case:** Minimum testing errors by level of noise and configuration - multi-step prediction.
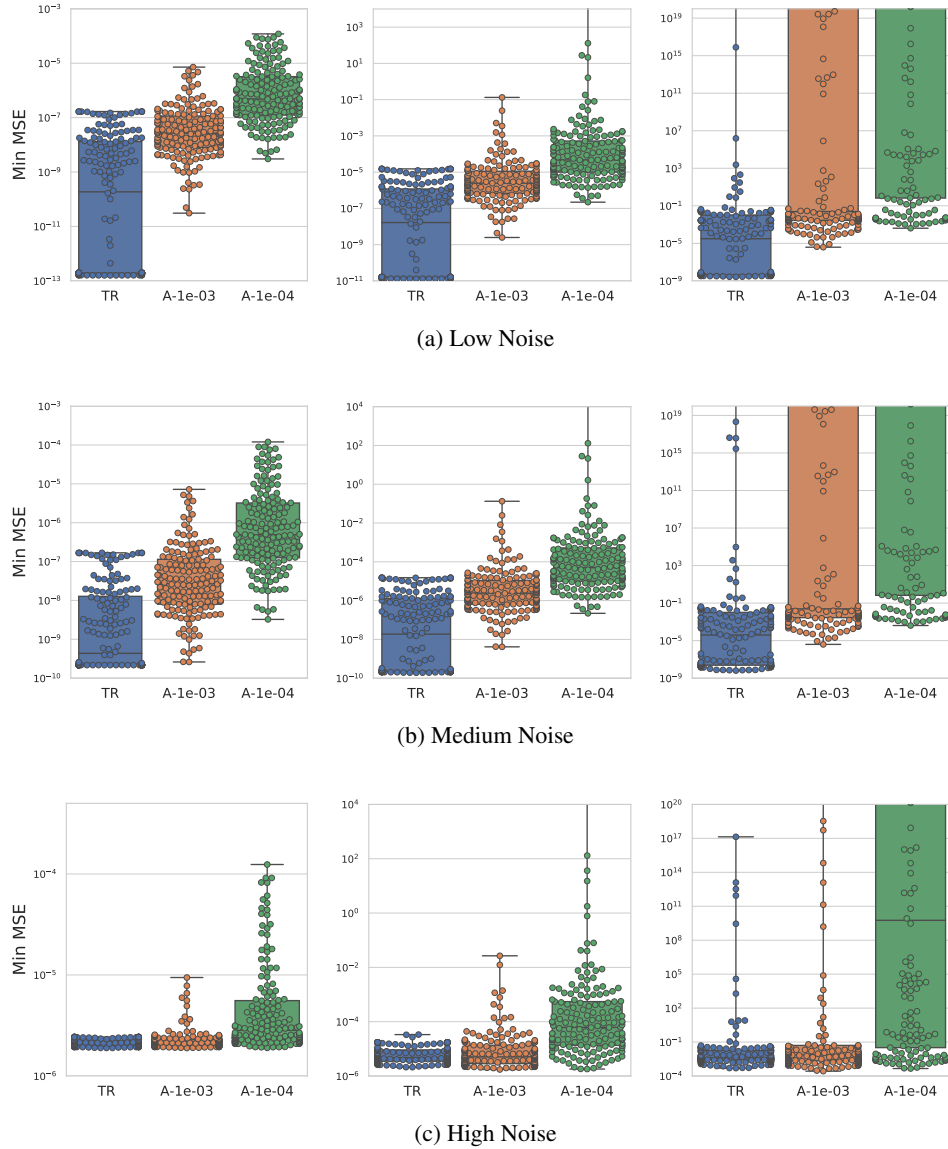
Figure 45: **Noisy Case:** The minimum testing errors of the one-step (left), multi-step (middle) and 1000-step (right) predictions (aggregated over all configurations) by level of noise.
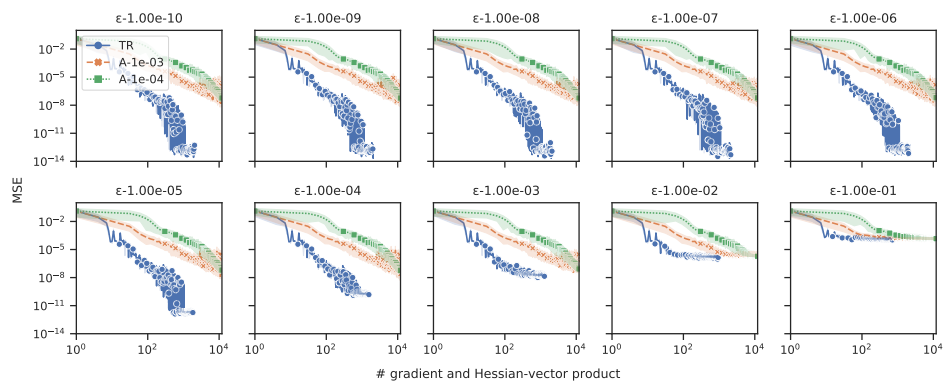
Figure 46: **Noisy Case:** Sensitivity analysis - the evolution of the MSE loss of stochastic mini-batch by level of noise.
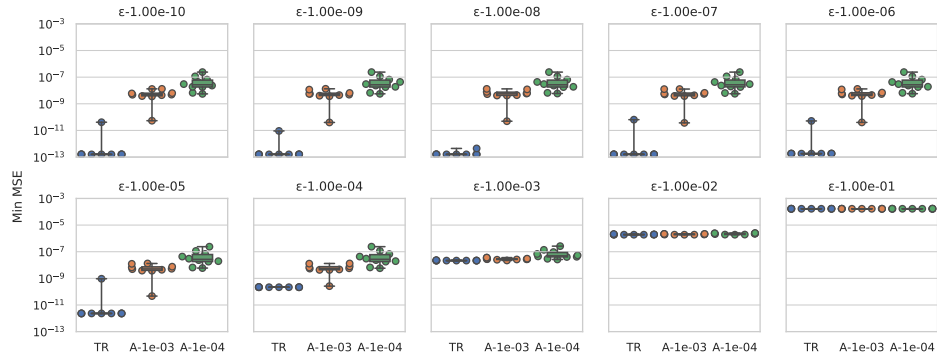
(a) One-Step Prediction
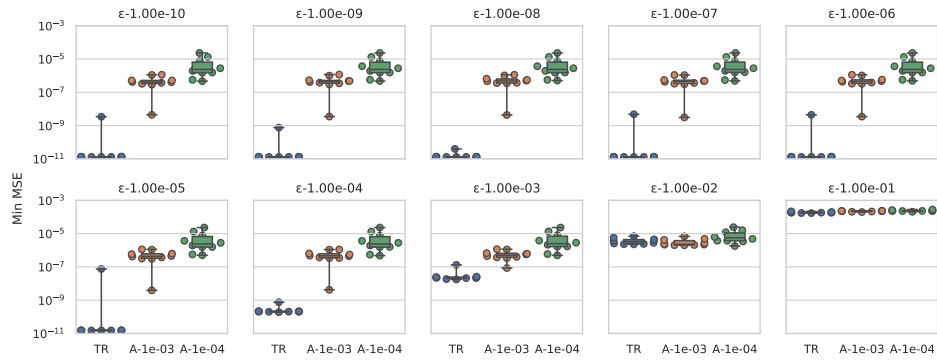
(b) Multi-Step Prediction
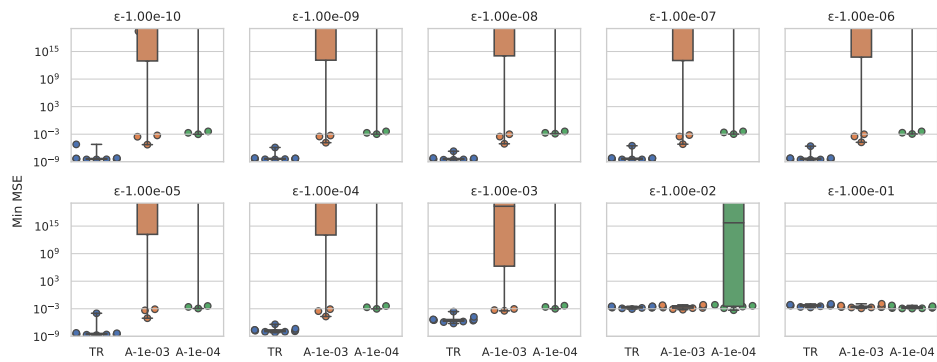
(c) 1000-Step Prediction

Figure 47: **Noisy Case:** Sensitivity analysis - the minimum testing errors by level of noise.
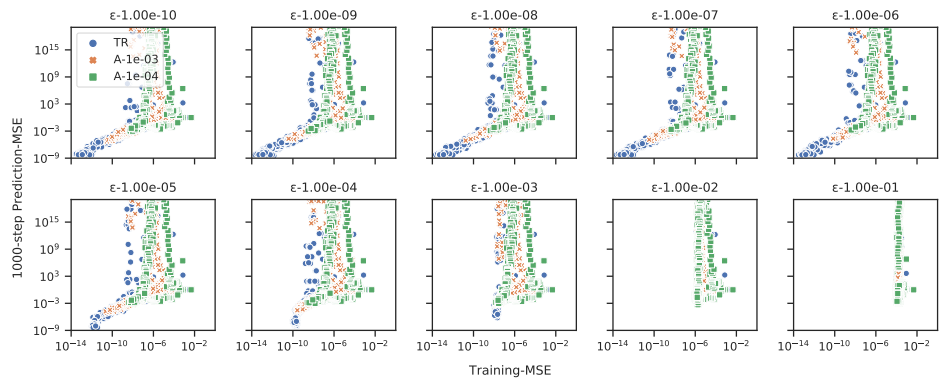
Figure 48: **Noisy Case:** Sensitivity analysis - training vs. 1000-step prediction (over the training process) by level of noise.